

# Analytical Performance Evaluation of Quantum Radar Architectures: From Single-Photon to Entangled-Noise Radars

H. Allahverdi<sup>1,2</sup> and Ali Motazedifard<sup>3,1, a)</sup>

<sup>1)</sup>Quantum Remote Sensing Lab, Quantum Metrology Group, Iranian Center for Quantum Technologies (ICQT), Tehran, Tehran 15998-14713, Iran

<sup>2)</sup>Laser and Plasma Research Institute, Shahid-Beheshti University, Tehran, Tehran 19839-69411, Iran

<sup>3)</sup>Department of Physics, University of Tehran, Tehran 14395-547, Iran

(\*Electronic mail: [alimotazedifard@ut.ac.ir](mailto:alimotazedifard@ut.ac.ir).)

(Dated: 10 June 2026)

This article presents a comprehensive analysis of two classes of quantum radars, including quantum direct-detection and quantum-entangled noise radars. In the first case, inspired by the well-established concept of single-photon LiDARs, we investigated the performance of single-photon radars, in which state-of-the-art single microwave-photon detectors are employed to enhance the detection sensitivity and enable the detection of weaker signals. We derived analytical expressions for the maximum detection range of both classes of quantum radars in terms of the Lambert W function, by considering all relevant system, target, and environmental parameters. Our formulation facilitates direct comparison of noise radars with direct-detection radars, and suggests that a quantum-entangled noise radar can be regarded as an enhanced direct-detection radar with an *effective threshold signal-to-noise ratio*. Furthermore, we applied this framework to classical-correlated noise radars and defined the parameter *range enhancement factor* (REF) to quantify the superiority of quantum-entangled noise radars over their classical counterparts. Moreover, we introduced a rule-of-thumb for approximating the REF. We also examined the influence of limitations imposed by various microwave detection technologies. Our analysis shows that the conventional antennas limit the potential benefits of quantum-entangled noise radar systems. We also demonstrated that the optimal detection method for these radars is a microwave detector based on a quantum transducer combined with a single optical-photon detector. We showed that, with the current technology, implementing a quantum-entangled noise radar with the maximum detection range in the order of few kilometers is possible. Finally, we explored the potential applications of quantum-entangled noise radars.

## I. INTRODUCTION

The detection and characterization of nearby objects using microwave electromagnetic (EM) fields—commonly referred to as RADAR (Radio Detection and Ranging)—originated from the pioneering work of the German physicist Heinrich Hertz<sup>1</sup>. The operating principle of radar is conceptually straightforward: a microwave signal is transmitted toward a region where a target may be present, and the returned signal is analyzed to determine the presence of the target and estimate its characteristics, such as an image, range, azimuth, and velocity. Nowadays, radar systems are widely employed across various domains, including biomedical sensing<sup>2,3</sup>, space and CubeSat technologies<sup>4</sup>, navigation<sup>5</sup>, aviation safety<sup>6</sup>, and smart wearable devices<sup>7</sup>.

The traditional radar systems—often referred to as direct-detection radars—rely on the analysis of the received signal power,  $P_r$ , as the detection function<sup>8</sup>. However, their performance can be degraded significantly in the presence of unwanted interference, such as environmental thermal noise and external microwave signals at similar frequencies. To mitigate these challenges, engineers have introduced an alternative strategy: store a reference copy of the transmitted signal (known as the idler) and compare it with the received signal<sup>9–12</sup>. These systems, which are well-known as noise radars, utilize the cor-

relation between the received signal and the retained idler as the detection function. A stronger correlation yields more accurate target detection or a larger practical radar range under the same conditions and system parameters. This leads to a fundamental question: *What is the ultimate limit of signal-idler correlation in noise radar systems?* From the classical standpoint, the maximum correlation occurs when the transmitted signal and the retained idler share identical waveforms<sup>9</sup>, differing only in their quantum fluctuations which remain distinct. However, a quantum mechanical solution to achieve correlations that exceed classical bounds is exploiting a pair of entangled electromagnetic fields as the signal-idler modes<sup>13–15</sup>. This is at the heart of the quantum illumination (QI) protocol<sup>16</sup>. Note that in the case of entangled state signals, not only their mean fields (in the X- or P-quadrature) are quantum mechanically correlated, but their zero-point quantum fluctuations are also inherently correlated. This leads to stronger correlations than those achievable by any classically correlated signals.

The first experimental demonstration of QI was achieved in the optical domain using bulk nonlinear optics<sup>17</sup>. In this experiment, a 6 dB improvement in the error-probability exponent over the best classical strategy was demonstrated. The extension of QI to the microwave domain was proposed recently<sup>18</sup>, where an electro-opto-mechanical system was proposed for generating entangled microwave–optical photon pairs. Despite its advantages, the original QI protocol requires a *joint* measurement of the returned signal and the retained idler. This approach becomes impractical in radar systems where the target range (and thus the signal’s arrival time) is unknown. For

<sup>a)</sup><https://profile.ut.ac.ir/~alimotazedifard/network>

this reason, the system proposed in Ref.<sup>18</sup> is not directly suitable for radar applications. The experimental demonstration of the first microwave QI-inspired radar that does not require joint measurement was shown in Refs.<sup>19,20</sup>. The implemented system, which is known as the quantum two-mode squeezed (QTMS) radar, utilizes a Josephson Parametric Amplifier (JPA) cooled to below 10 mK in a cryostat to generate entangled microwave signals at GHz frequencies.

In recent years, significant theoretical and experimental progress has been made in the field of quantum illumination (QI), both in the optical domain<sup>21–30</sup> and in microwave QTMS radar systems<sup>31–34</sup>. Most of the existing works on microwave QI have focused on the enhancement of signal-idler correlations via entanglement and by improving system performance, for example, by considering receiver operating characteristic (ROC) curves, detection signal-to-noise ratio (SNR), and measurement time. However, despite their importance, these metrics are not sufficient to evaluate the practical performance of such radar systems in long-range detection scenarios. A more comprehensive analysis rooted in range-dependent system behavior is required.

A standard method to evaluate the maximum range at which a QTMS radar can detect a target is through a range equation that expresses the signal-idler correlation as a function of target range,  $R$ . In Ref.<sup>35</sup>, an explicit expression for the Pearson correlation coefficient  $\rho$  as a function of range  $R$  for noise radar systems was derived. The formulation introduced in Ref.<sup>35</sup>, despite its novelty, overestimated the Pearson correlation coefficient of the generated entangled signal-idler fields. It is valid in the special case where an RF amplifier used to amplify the signal and idler modes adds substantial noise. This condition is not satisfied in QI experiments, since they usually employ low-noise amplifiers. Moreover, their analysis neglects key real-world parameters, such as atmospheric absorption and detection time. The latter is important for moving objects, while absorption becomes practically important in long-range applications. These omissions compromise the validity of the range estimation based on the formulation proposed in<sup>35</sup>, leading to an overestimation of the system's operational performance.

Some recent studies<sup>36–39</sup> have attempted to estimate the maximum detection range of quantum-entangled noise radars using the classical radar range equation that was developed for direct-detection radar systems. These models assume power of the received signal as the detection function. This assumption is fundamentally inconsistent with the operational principle of quantum radars, where the signal-idler correlation—not the signal power—acts as the primary detection function. Additionally, these works neglect atmospheric attenuation, which can significantly affect the validity of their results in long-range real-world applications.

Motivated by the above-mentioned investigations, in this paper, we aim to address these gaps by developing an analytical framework to evaluate the maximum detection range of quantum-entangled noise radars. Specifically, we derived a closed-form expression for the maximum detection range of continuous-wave (CW) quantum-entangled noise radars in terms of the Lambert  $W$  function. Our analysis takes into account the effects of atmospheric absorption, detection time, and

signal bandwidth. We also investigate how different microwave detection technologies affect the performance of quantum-entangled noise radars. Our approach extends and generalizes the analytical formulation presented in Ref.<sup>35</sup> to include these critical practical considerations. By utilizing this formulation, we showed that implementing a quantum-entangled radar system with a maximum detection range on the order of kilometers is achievable based on current technologies. Furthermore, we addressed strategies for overcoming the present limitations, such as increasing the entanglement strength, using single microwave-photon detectors (SMPDs), and most importantly, increasing the bandwidth of the generated entangled microwave fields. The latter is shown to significantly improve the quantum advantage by reducing the photon number per mode, thus enhancing the feasibility of long-range operation which is consistent with the recent experimental insights<sup>33,34</sup>. In addition, building upon recent advances in high-efficiency SMPDs, we proposed the concept of the single-photon radar (SPR), which is analogous to single-photon LiDARs.

The paper is organized as follows. In Sec. II, we review the range equation in conventional classical direct-detection radars. Here, we derived an analytical expression for maximum detection range and introduce the single-photon direct-detection radar in this context. We then introduce noise radars in Sec. III. Utilizing results obtained in Sec. III, we compare the performance of QTMS radars and classical noise radars in this section. Experimental discussion on the feasibility and comparison as well as addressing challenges are provided in this section. Finally, concluding remarks and outlooks for future works are discussed in Sec. IV.

## II. QUANTUM DIRECT-DETECTION RADARS

In this section, we first review the operational principles of direct-detection radars to provide an explicit expression for the maximum detection range of SPRs. This establishes a baseline for comparison with quantum-entangled noise radars.

### A. A Short Review on Principles of Direct Detection Radar Systems

Figure 1 illustrates the schematic diagram of a direct-detection radar system. The system begins with a digital signal generator producing an intermediate frequency (IF) signal. It is subsequently converted into an analog signal by a digital-to-analog converter (DAC). This analog signal is then up-converted to radio frequency (RF), amplified, and finally transmitted toward the target region via the radar transmitter antenna (Tx). The transmitted microwave signal, with power  $P_t$ , undergoes atmospheric attenuation before interacting with the target. A portion of this signal is back-scattered toward the radar receiver antenna (Rx). At the receiver, the back-scattered signal (with power  $P_r$ ) along with the environmental noise is first amplified and then down-converted to an intermediate frequency (IF). The signal then passes through an IF bandpass filter with bandwidth  $B_{IF}$  before being digitized by a high-

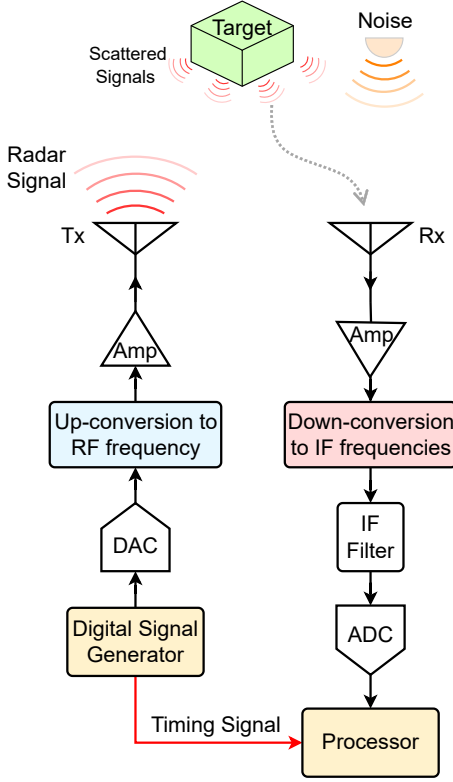


FIG. 1: The schematic diagram of a mono-static direct-detection radar system. Amp.: Amplifier; DAC: Digital-to-analog converter; ADC: Analog-to-digital converter; Tx/Rx: Transmitter/receiver microwave antenna.

speed analog-to-digital converter (ADC). The digitized signal is finally processed and interpreted by a digital processor (e.g., an FPGA). The relationship between the transmitted power  $P_t$  and the received power  $P_r$  is governed by the classical radar range equation, which is given by<sup>8</sup>

$$P_r = \eta(R)P_t, \quad (1)$$

in which  $\eta(R)$  is the transfer function of the transmitter-target-receiver channel and is given by<sup>8</sup>

$$\eta(R) = \frac{\sigma G A_e}{(4\pi)^2 R^4} F(R)^2. \quad (2)$$

In this equation,  $R$  is the range to the target,  $\sigma$  is the radar cross-section (RCS), and  $G$  represents the antenna gain. Moreover,  $A_e$  is the effective aperture of the receiver antenna and relates to the physical antenna aperture  $A$  via  $A_e = \epsilon_a A$ , with  $\epsilon_a$  being the antenna aperture efficiency. Finally,  $F(R) = 10^{-\gamma R/10}$  denotes the form factor describing the attenuation of the radar signal due to atmospheric absorption or loss, where  $\gamma$  is the atmospheric absorption coefficient in units of dB/m.

In addition to the portion of the radar signal back-scattered from the target, the radar receiver also collects unwanted signals from the environment, whose power we denote by  $P_n$ . When the target detection process is carried out over  $M$  independent measurements, the effective signal-to-noise ratio (SNR) for the direct-detection radar system is given by  $\text{SNR}_{\text{eff}}^{\text{DDR}} = MP_r/P_n = M\eta(R)P_t/P_n$ <sup>8</sup>. It is important to note that the number of measurements  $M$  depends on the integration time  $\tau_{\text{int}}$  and the detection bandwidth  $B_{\text{det}}$ , through the relation  $M = \tau_{\text{int}}B_{\text{det}}$ . The detection bandwidth itself is determined by the IF filter bandwidth  $B_{\text{IF}}$  at the receiver, i.e.,  $B_{\text{det}} = B_{\text{IF}}$ .

A direct-detection radar enables reliable identification of the target when the effective signal-to-noise ratio exceeds a predefined detection threshold, denoted as  $\text{SNR}_{\text{th}}$ . In other words, reliable detection occurs if and only if  $\text{SNR}_{\text{eff}}^{\text{DDR}} > \text{SNR}_{\text{th}}$ , which is commonly referred to as the detection criterion<sup>8</sup>. Note that the threshold SNR refers to the minimum required power of the returned radar signal,  $P_{r,\text{min}}$ , or, equivalently, the minimum detectable signal (MDS), for which the radar system is capable of recognizing the presence of the target. This leads to  $\text{SNR}_{\text{th}} = P_{r,\text{min}}/P_n$ . For instance, for a typical radar system with  $\text{SNR}_{\text{th}} = 10$  dB, the power of the returned signal  $P_r$  should be at least 10 dB higher than environmental noise power  $P_n$  so that the radar system is able to identify the target, i.e.,  $P_r$  (dB)  $\geq P_n$  (dB) + 10 dB, or equivalently,  $P_r$  (SI)  $\geq 10 \times P_n$  (SI).

By substituting the direct detection radar range equation given by Eq. 1 in the detection criterion, and considering that the equality in the detection criterion holds for the maximum detection range of the radar system  $R_{\text{max}}$ , one can get to

$$R_{\text{max}} \exp\left(\frac{\ln(10)}{20} \gamma R_{\text{max}}\right) = \left(\frac{M}{\text{SNR}_{\text{th}}}\right)^{1/4} R_c^{(\text{DDR})}. \quad (3)$$

Here,  $R_c$  is the characteristic-range of the direct detection radar system and defined as

$$R_c^{(\text{DDR})} \equiv \left(\frac{\sigma G A_e P_t}{(4\pi)^2 P_n}\right)^{1/4}. \quad (4)$$

$R_c^{\text{DDR}}$  is the range for which the total power at the receiver for in-vacuo signal propagation ( $\gamma = 0$ ) is 3 dB above the noise level, or equivalently, twice the noise power  $P_n$ . Alternatively, it can be interpreted as the range for which the SNR at the receiver equals 1 (or 0 dB). The characteristic range depends on the radar system parameters, the transmitted signal power  $P_t$ , and the environmental thermal noise power  $P_n$  which is given by<sup>8</sup>

$$P_n = N_b h f B_{\text{det}}. \quad (5)$$

In this equation,  $N_b = [\exp(hf/k_B T) - 1]^{-1}$  is the mean photon number of the background thermal noise per mode,  $f$  denotes the signal frequency. Moreover,  $h = 6.63 \times 10^{-34}$  J.s is the Planck constant,  $k_B = 1.38 \times 10^{-23}$  J.K is the Boltzmann constant, and  $T$  denotes the environmental temperature. For instance, for  $f = 10$  GHz,  $T = 300$  K, and  $B_{\text{det}} = 200$  kHz, we have  $N_b \simeq 624$  and  $P_n \simeq -120.82$  dBm.

Equation (3) can be analytically solved to obtain an explicit expression for  $R_{\max}$ . The solution of Eq. (3) can be represented in term of the Lambert W-function as follows<sup>40,41</sup>

$$R_{\max}^{(\text{DDR})} = \frac{20}{\ln(10)\gamma} W_0 \left[ \frac{\ln(10)}{20} \gamma \left( \frac{M}{\text{SNR}_{\text{th}}} \right)^{1/4} R_c^{(\text{DDR})} \right], \quad (6)$$

in which  $W_0(x)$  denotes the principal branch of the Lambert's W function, which is a real and increasing function for  $x \geq -1/e$ . This equation determines the maximum detection range of a conventional direct detection radar in terms of the system and environmental parameters. Several key insights can be understood from this expression: the maximum detection range can be increased by decreasing of the atmospheric absorption coefficient  $\gamma$ , and by increasing of the transmitted signal power  $P_t$  and the integration samples number  $M$ .

Equation (6) demonstrates that for a given transmit power  $P_t$ , a critical factor influencing the maximum detection range is the threshold signal-to-noise ratio required for target detection. This threshold depends on the sensitivity of the microwave detector and the specific detection strategy employed in the radar receiver. Conventional direct-detection radars typically operate with  $\text{SNR}_{\text{th}}$  values in the range of 10–20 dB<sup>8</sup>. By utilizing recently developed high-efficiency SMPDs at the radar receiver,  $\text{SNR}_{\text{th}}$  can be significantly reduced. Analogous to the well-known single-photon LiDARs, we refer to this class of direct-detection radars that utilize SMPDs at their receivers as single-photon radars (SPRs). This improvement and its implications will be discussed in the following sections.

## B. The Single-Photon Radar Idea

As demonstrated previously, the threshold SNR of the radar receiver plays a critical role in determining the maximum detection range of a direct-detection radar. The development of SMPDs, which offer enhanced sensitivity, provides a substantial reduction of  $\text{SNR}_{\text{th}}$ . This, in turn, extends the operational range of conventional direct-detection radars substantially. Note that this is important in scenarios where traditional radars have a limited range due to low transmit power. In these cases, SPRs can operate effectively as covert radars. The idea of the SPR is similar to single-photon LiDAR, which utilizes single optical-photon detectors (SOPDs) in the LiDAR receiver<sup>49</sup>. While SMPDs are not yet commercially available, substantial progress has been made toward their development. Existing implementations of SMPDs have so far been demonstrated only as a proof-of-concept in laboratory environments<sup>42–47</sup>.

Despite their promise, implementing single-photon detection in the GHz frequency range is technically challenging due to the fact that photon energy is approximately five orders of magnitude lower than that of optical photons. However, in Ref.<sup>45</sup>, an SMPD is implemented using an impedance-matched artificial  $\Lambda$  system comprising the dressed states of a driven superconducting qubit coupled to a microwave resonator. This SMPD achieved a high single microwave-photon detection efficiency of  $0.66 \pm 0.06$ , with a low dark-count probability of  $0.014 \pm 0.001$  at  $\sim 10$  GHz frequency. Also, in Ref.<sup>46</sup> an SMPD with an efficiency of 70% in the frequency range of

3–5.2 GHz is realized based on a hybrid system comprising a double quantum dot charge qubit electrostatically defined in a GaAs/AlGaAs heterostructure, coupled to a high-impedance Josephson junction array cavity. Moreover, in Ref.<sup>42</sup>, an SMPD based on a superconducting transmon qubit with a detection efficiency of 0.8 at the frequency of 7 GHz, and with the dark-count rate (DCR) below 30 counts per second (cps) is reported. In addition, in Ref.<sup>43</sup>, a bolometric SMPD based on the irreversible photon absorption by a transmon qubit via a four-wave-mixing process is demonstrated with quantum efficiency about 45% near the frequency of 7 GHz. The features of some implemented SMPDs are summarized in Table I. It is worth noting that the sensitivity of classical receiver antennas is in the range of  $10^{-13}$ – $10^{-18}$  W/ $\sqrt{\text{Hz}}$ , which is about one to five orders of magnitude greater than SMPDs.

The technological advances in single microwave-photon detection suggest a novel class of quantum direct-detection radars as single-photon microwave radars, analogous to single-photon terahertz radars and LiDARs<sup>48,49</sup>. An important aspect of this analogy is that all signal-processing techniques previously developed for single-photon LiDARs, such as time-correlated single-photon counting (TCSPC) or photon-statistical analysis<sup>50</sup>, are now applicable to single-photon microwave radars. These processing techniques can efficiently reduce the threshold SNR required for target detection, leading to radar-signal identification at SNR levels as low as approximately  $-40$  dB, whereas it is about 10–20 dB for classical direct-detection radar systems.

To illustrate the impact of the threshold SNR, in Fig. 2a we have plotted the maximum detection range of a direct-detection radar,  $R_{\max}$ , as a function of the transmitted signal power,  $P_t$ , and the corresponding photon rate,  $R_t = P_t/hf$ , for various threshold SNR from  $-40$  dB to  $+20$  dB. In this figure, the system parameters are  $f = 10$  GHz,  $\sigma = 0.5$  m<sup>2</sup>,  $G = 15$  dB,  $\epsilon_a = 0.5$ ,  $A = 0.01\pi$  m<sup>2</sup>,  $T = 300$  K,  $\tau_{\text{int}} = 100$  ms,  $B_{\text{det}} = 200$  kHz, and  $\gamma = 0.007$  dB/km<sup>51</sup>. As expected, the maximum detection range increases by increasing the transmit power. However, for a fixed  $P_t$ , the maximum detection range also increases by decreasing the threshold SNR. For example, with a transmit power of  $P_t = 1$  nW, which corresponds to the photon rate of  $R_t = 1.5 \times 10^{14}$  cpp (counts per pulse), the detection range is approximately 2.9 m at  $\text{SNR}_{\text{th}} = 20$  dB (dotted red line). However, this range increases to nearly 80 m when the threshold SNR is reduced to  $-40$  dB (dashed red line). In the high-brightness regime, with  $P_t = 1$  mW, which corresponds to a photon rate of  $R_t = 1.5 \times 10^{20}$  cpp, the maximum detection range is approximately 79.5 m for  $\text{SNR}_{\text{th}} = 20$  dB, while it is about 2480 m when the threshold SNR is decreased to  $-40$  dB.

One critical consideration in the operation of single-photon microwave radars is whether a sufficient number of signal photons returned to the receiver for detection or not. It is important especially when the power of the transmitted signal is extremely weak. To address this, we compare the power (or the photon rate) of the received signal with the minimum detectable signal (MDS), which is given by

$$P_{\text{MDS}} = \frac{1}{M} \text{SNR}_{\text{th}} \times P_n, \quad (7)$$

TABLE I: Summary of selected single microwave-photon detectors demonstrated to date.

	Frequency (GHz)	Efficiency (%)	Dark count rate / Probability (cps) / -	Bandwidth (MHz)	Dead time (ns)	Sensitivity (W/ $\sqrt{\text{Hz}}$ )	Year
42	7	80	30 cps	0.1-1	-	$3 \times 10^{-23}$	2025
43	7	43	85 cps	1	-	$10^{-22}$	2024
44	10.220	96	$0.030 \pm 0.002$	20	4500	-	2020
45	10	66	$0.014 \pm 0.001$	16	400	-	2016
46	3–5.2	70	-	-	3	$5 \times 10^{-19}$	2025
47	6.042	73	167 kcps	0.7	3000	$3.228 \times 10^{-21}$	2024

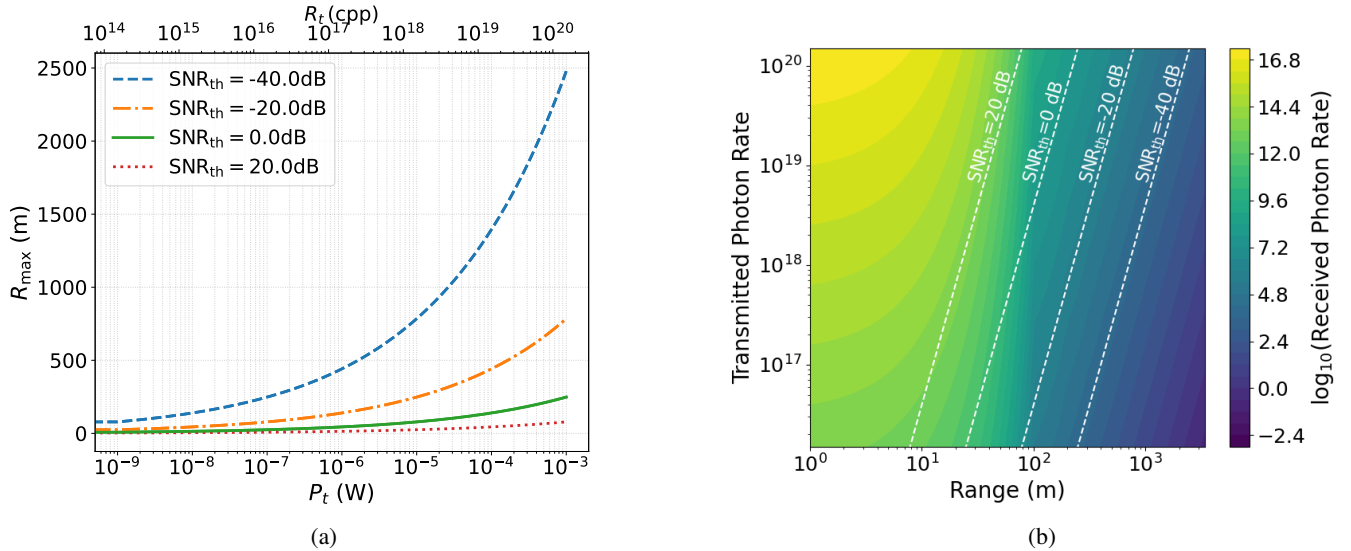


FIG. 2: (color online) (a) The maximum detection range of the direct detection radar versus the transmitted signal power  $P_t$  (lower horizontal axis) and its relevant transmitted photon rate  $R_t = P_t/(hf)$  (upper horizontal axis) in the high brightness regime for the different values of the threshold SNR as  $\text{SNR}_{\text{th}} = \{-40, -20, 0, 20\}$  dB. (b) Contour plot describing the photon rate of the received signal versus the target range  $R$  and the photon rate of the transmitted signal  $R_t = P_t/hf$ . The white-dashed lines in this figure represents the *minimum* transmitted photon rate required for resolving the target at range  $R$  for the fixed values of  $\text{SNR}_{\text{th}}$ . The transmitted signals with powers under these curves are not sufficient for detecting the target with the considered threshold SNR. The other system parameters are as  $f = 10$  GHz,  $\sigma = 0.5$  m<sup>2</sup>,  $G = 15$  dB,  $\epsilon_a = 0.5$ ,  $A = 0.01\pi$  m<sup>2</sup>,  $T = 300$  K,  $\tau_{\text{int}} = 100$  ms,  $B_{\text{det}} = 200$  kHz, and  $\gamma = 0.007\text{dB/km}$ <sup>51</sup>.

where  $M$  is the number of integration samples, and  $P_n$  is the noise power. Note that the detection occurs only if  $P_r \geq P_{\text{MDS}}$ , which is consistent with the detection criterion described in Sec. II A. By substituting the expression for the power of the received signal,  $P_r$ , from Eq. (1), into this inequality, we obtain

$$P_t \geq \frac{\text{SNR}_{\text{th}} \cdot P_n}{M \cdot \eta(R)}. \quad (8)$$

This relation defines the minimum power (or the photon rate) of the transmitted signal for which the power of the received signal exceeds the MDS.

Figure 2b shows the received photon rate,  $R_r = P_r/hf$ , as a function of the transmitted photon rate,  $R_t = P_t/hf$ , and the target range  $R$ . In this figure, the white-dashed lines indicate the *minimum* transmitted photon rate that is required to detect the target at given range for each value of  $\text{SNR}_{\text{th}}$ . If the transmitted photon rate falls below the respective threshold curve, the

photon rate of the received signal will be less than the MDS, and thus, the detection of target is no longer possible. Also, this figure shows that for  $\text{SNR}_{\text{th}} = 20$  dB, when the transmitter emits signal photons with the rate of  $1.5 \times 10^{20}$  cpp (equivalent to about  $\sim 1$  mW), the system is able to identify targets at ranges up to 77 m. In this case, the photon rate of the received signal is approximately  $\sim 10^{12}$  cpp. Moreover, for  $\text{SNR}_{\text{th}} = -40$  dB, the transmitted signal photon rate should be at least  $4 \times 10^{18}$  cpp (equivalent to  $15 \mu\text{W}$ ) in order to detect targets at the range of 1 km. Under this condition, the photon rate of the received signal is greater than  $\sim 10^{3.6}$  cpp.

### III. QUANTUM-ENTANGLED NOISE RADARS

In direct-detection radars, the returned signal can be easily masked by a noise source or unwanted signals incident on

the receiver. To overcome this limitation, it is proposed to extract the desired signal from the noise by correlating the received signal with the reference signal, which is a copy of the transmitted signal.<sup>9–12</sup> This is the main operational principle of noise radar systems.

The simplified schematic diagram of a noise radar is shown in Fig. 3. In this system, a pair of correlated fields, either classical or quantum, is generated by the microwave source. One of these fields, referred to as the signal, is amplified and then transmitted toward the target region. However, the other one, known as the idler, is amplified, detected, and recorded as the reference. This reference is later used to distinguish the desired signal from unwanted noise in the received field via correlation. At the receiver, the received signal, which may include the back-scattered signal (if the target is present) along with various noise contributions, is detected. It is then amplified and down-converted to an IF frequency in the radar base-band. After that, it is filtered and digitized using a high-sample-rate, high-bandwidth analog-to-digital converter (ADC). The target information is then extracted through a process known as matched filtering<sup>52</sup>.

It is important to note that a key difference between the classical and quantum noise radars is their microwave source used to generating correlated signal-idler fields. In the classical case, the signal and idler are classically correlated electromagnetic (EM) fields. In contrast, in the quantum case, the signal and idler are entangled EM waveforms, meaning that the corresponding quantum state shows strong non-classical correlations<sup>16,18,52</sup>.

In noise radars, the degree of correlation between the signal and idler fields is typically quantified using the covariance matrix constructed from the in-phase ( $I$ ) and quadrature ( $Q$ ) voltage components of the fields. This matrix is defined as follows<sup>53,54</sup>

$$\text{Cov} = \begin{pmatrix} C_{SS} & C_{SI} \\ C_{IS} & C_{II} \end{pmatrix}, \quad (9)$$

where  $C_{nm}$  ( $n, m \in \{S, I\}$ ) is a  $2 \times 2$  block, and given by

$$C_{nm} = \frac{\langle \hat{I}_n \hat{I}_m \rangle}{\langle \hat{Q}_n \hat{I}_m \rangle} \frac{\langle \hat{I}_n \hat{Q}_m \rangle}{\langle \hat{Q}_n \hat{Q}_m \rangle}. \quad (10)$$

Here,  $\langle \cdot \rangle$  denotes the quantum expectation value, and the operators  $\hat{I}_k$  and  $\hat{Q}_k$  represent the quantum-mechanical in-phase and quadrature voltage components of the electromagnetic field, respectively, which defined as

$$\hat{I}_k = \frac{1}{\sqrt{2}}(\hat{a}_k + \hat{a}_k^\dagger), \quad (11)$$

$$\hat{Q}_k = \frac{1}{i\sqrt{2}}(\hat{a}_k - \hat{a}_k^\dagger), \quad (12)$$

where  $\hat{a}_k$  and  $\hat{a}_k^\dagger$  are the annihilation and creation operators, respectively, associated with the mode  $k$ , with  $k = S$  for the signal and  $k = I$  for the idler mode.

The off-diagonal blocks of the covariance matrix, namely  $C_{SI}$  and  $C_{IS}$ , represent the correlations between the in-phase ( $I$ ) and quadrature ( $Q$ ) voltage components of the signal and idler fields. The strength of this correlation is quantified by

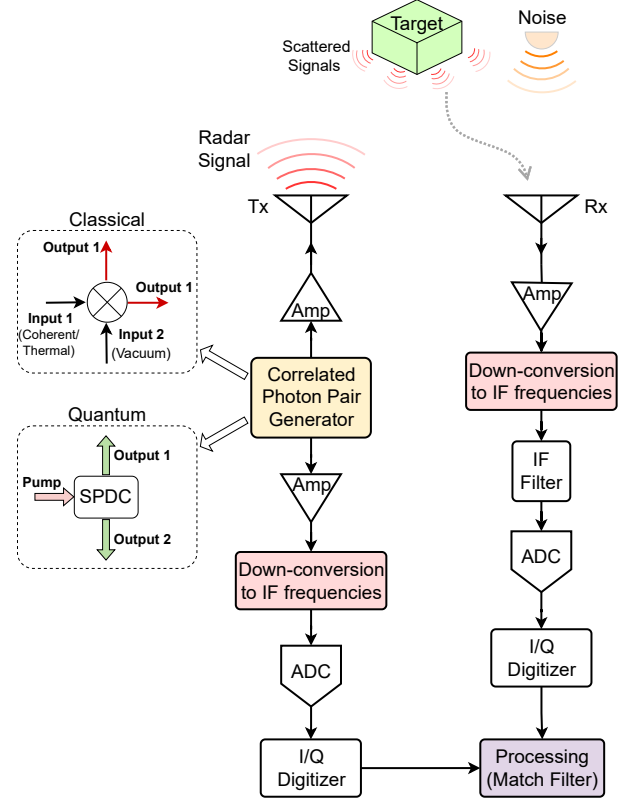


FIG. 3: The schematic diagram of a mono-static noise radar system. Amp.: Amplifier; ADC: Analog to digital converter; SPDC: Spontaneous parametric down-conversion.

the well-known Pearson correlation coefficient,  $\rho$ , which is defined as

$$\rho = \frac{\langle \hat{I}_S \hat{I}_I \rangle}{\sqrt{\langle \hat{I}_S^2 \rangle \langle \hat{I}_I^2 \rangle}}. \quad (13)$$

Conceptually, the role of the Pearson correlation coefficient,  $\rho$ , in noise radars is analogous to that of the signal power in direct detection radars. It is the detection function that indicates the presence of the target within the interrogation region<sup>55</sup>, as discussed in Sec. II. Under the target-present hypothesis ( $H_1$ ), a nonzero correlation exists between the received signal and the retained idler, i.e.,  $\rho \neq 0$ . Conversely, when there is no target (hypothesis  $H_0$ ), the correlation disappears, i.e.,  $\rho = 0$ .

To calculate the correlation coefficient between the *detected* signal (at the receiver) and idler fields quantum mechanically using Eq. (13), it is necessary to determine the annihilation operators corresponding to the detected signal and idler fields in terms of the system and environmental parameters. For the signal field, the annihilation operator of the detected field

depends on the presence of the target, which is given by

$$H_1 : \hat{a}_{S,1}^{\text{det}} = \sqrt{\eta(R)G_S}\hat{a}_S + \hat{a}_{S,\text{add}}^{(1)}, \quad (14)$$

$$H_0 : \hat{a}_{S,0}^{\text{det}} = \hat{a}_{S,\text{add}}^{(0)}. \quad (15)$$

Here,  $\hat{a}_{S,\text{add}}^{(1)}$  and  $\hat{a}_{S,\text{add}}^{(0)}$  refer to the annihilation operator of the noise added to the signal that reaches to the receiver under  $H_1$  and  $H_0$  hypotheses, respectively, which are given by

$$\hat{a}_{S,\text{add}}^{(1)} = \sqrt{[1-\eta(R)]G_{S,\text{rec}}}\hat{a}_{\text{env}} + \sqrt{\eta(R)G_{S,\text{rec}}}\hat{L}_{S,\text{tr}}^\dagger + \hat{L}_{S,\text{rec}}^\dagger, \quad (16)$$

$$\hat{a}_{S,\text{add}}^{(0)} = \sqrt{G_{S,\text{rec}}}\hat{a}_{\text{env}} + \hat{L}_{S,\text{rec}}^\dagger. \quad (17)$$

In these relations,  $G_S = G_{S,\text{rec}}G_{S,\text{tr}}$  is the total amplification gain of the signal,  $G_{S,\text{tr}}$  and  $G_{S,\text{rec}}$  denote the signal gains at the transmitter and receiver, respectively. Moreover,  $\hat{a}_{\text{env}}$  gives the annihilation operator of the thermal background noise. In addition,  $\hat{L}_{S,\text{tr}}$  and  $\hat{L}_{S,\text{rec}}$  denote the Langevin noise operators that describe the noise added to the fields through the RF amplifiers at the transmitter and receiver, respectively, such that<sup>56</sup>

$$\hat{L}_{S,\text{tr}} = \sqrt{G_{S,\text{tr}}-1}\hat{c}_{S,\text{tr}}, \quad (18)$$

$$\hat{L}_{S,\text{rec}} = \sqrt{G_{S,\text{rec}}-1}\hat{c}_{S,\text{rec}}. \quad (19)$$

Here,  $\hat{c}_{S,\text{tr}}$  and  $\hat{c}_{S,\text{rec}}$  are bosonic field operators satisfying the commutation relation  $[\hat{c}_k, \hat{c}_k^\dagger] = 1$ . It should be noted that the mean photon number of the noise added through the RF amplifier is given by

$$N_k^{\text{amp}} \equiv \langle \hat{c}_k^\dagger \hat{c}_k \rangle = k_B T_{\text{eff},k} (10^{\text{NF}_k/10} - 1) / hf_k \quad (20)$$

in which  $T_{\text{eff},k}$  is the effective temperature of the amplifier,  $\text{NF}_k$  denotes its noise figure in dB scale,  $f_k$  is the frequency, and  $k \in \{(S, \text{rec}); (S, \text{tr}); I\}$  is dummy index.

The annihilation operator of the detected idler mode is independent of the target presence, and given by

$$\hat{a}_I^{\text{det}} = \sqrt{G_I}\hat{a}_I + \hat{L}_I^\dagger, \quad (21)$$

in which  $G_I$  is the Idler amplification gain, and  $\hat{L}_I = \sqrt{G_I-1}\hat{c}_I$ .

The radar range equation for noise radars should establish a relationship between the correlation coefficient,  $\rho$ , and the target range,  $R$ . In the following, we present a comprehensive and explicit formulation of the range equation for both classical and quantum noise radars.

### A. Maximum Detection Range of Quantum-Entangled Noise Radar

In quantum-entangled noise radars, a microwave quantum two-mode squeezed vacuum (TMSV) state of the electromagnetic field (see Appendix. A) is employed as the quantum-correlated signal-idler pairs. In the number-state basis, the TMSV state is given by<sup>57,58</sup>

$$|\Psi\rangle_{\text{TMSV}} = \sum_{n=0}^{\infty} \sqrt{\frac{N_S^n}{(N_S+1)^{n+1}}} |n\rangle_S |n\rangle_I, \quad (22)$$

in which  $N_S$  is the average number of photons per mode, that relates to the transmitted power by  $P = hfN_S B$ , with  $f$  and  $B$  denoting the field frequency and the source bandwidth, respectively. Under the hypothesis  $H_1$ , the quantum state of the received signal and idler pair is described by the density matrix  $\hat{\rho} = \hat{\rho}_{SI} \otimes \hat{\rho}_{n,S} \otimes \hat{\rho}_{n,I}$ , such that  $\hat{\rho}_{SI} = |\Psi_{SI}\rangle \langle \Psi_{SI}|$  represents the density matrix of the correlated signal-idler pair, and  $\hat{\rho}_{n,k}$  refers to the density matrices of the noise added to the mode  $k \in \{S, I\}$ . Using this expression, one can calculate the terms appeared in the Pearson correlation coefficient (Eq. 13) as follows

$$\langle \hat{I}_S^2 \rangle_{\text{QI}} \simeq \eta(R)G_S \left( N_S + \frac{1}{2} \right) + N_{S,\text{add}}^{(1)}, \quad (23)$$

$$\langle \hat{I}_I^2 \rangle_{\text{QI}} \simeq G_I \left( N_S + \frac{1}{2} \right) + N_{I,\text{add}}, \quad (24)$$

$$\langle \hat{I}_S \hat{I}_I \rangle_{\text{QI}} = \sqrt{\eta(R)G_S G_I N_S (N_S + 1)}. \quad (25)$$

In these relations,  $N_{S,\text{add}}^{(1)}$  and  $N_{I,\text{add}}$  represent the mean photon number of the noise added to the signal and idler modes, respectively, and assumed to be very large compared to the zero-point fluctuations in the signal and idler noise modes. Using Eqs. 16 and 21, one can calculate the mean photon number of the added noise under the hypothesis  $H_1$  as follows

$$N_{S,\text{add}}^{(1)} = [1-\eta(R)]G_{S,\text{rec}}N_{\text{env}} + (G_{S,\text{rec}}-1)(N_{S,\text{rec}}^{\text{amp}}+1) + \eta(R)G_S(G_{S,\text{tr}}-1)(N_{S,\text{tr}}^{\text{amp}}+1), \quad (26)$$

$$N_{I,\text{add}} = (G_I-1)(N_I^{\text{amp}}+1). \quad (27)$$

Assuming that the RF amplifier in the radar transmitter affects the signal and idler modes equally (i.e.,  $G_{S,\text{tr}} \approx G_I$  and  $N_{S,\text{tr}}^{\text{amp}} \approx N_I^{\text{amp}}$ ), and  $\eta(R) \ll 1$  (which is the case of very low-reflecting objects in long ranges), one can rewrite  $N_{S,\text{add}}^{(1)}$  as follows

$$N_{S,\text{add}}^{(1)} = \eta(R)G_{S,\text{rec}}N_{I,\text{add}} + N_n, \quad (28)$$

in which

$$N_n \simeq G_{S,\text{rec}}N_{\text{env}} + (G_{S,\text{rec}}-1)(N_{S,\text{rec}}^{\text{amp}}+1). \quad (29)$$

In these relations,  $N_{\text{env}} = [\exp(hf/k_B T_{\text{env}}) - 1]^{-1}$  being the mean photon number of the environmental thermal noise. By substituting the results obtained in Eqs. (23)-(25) into Eq. (13), after some algebraic calculations, one can obtain the Pearson correlation coefficient as follows

$$\rho_{\text{QI}}(R) = \frac{\tilde{\rho}_0^{\text{QI}}}{\sqrt{1 + \frac{1}{\eta(R)G_{S,\text{rec}}} \frac{N_n}{\langle \hat{I}_I^2 \rangle}}}. \quad (30)$$

Here,  $\tilde{\rho}_0^{\text{QI}}$  represents the modified Pearson correlation coefficient between the signal and idler modes at the source (i.e., at  $R=0$ ), and is given by

$$\tilde{\rho}_0^{\text{QI}} = \sqrt{\rho_0^2 - \xi^2}, \quad (31)$$

with

$$\rho_0 = 1 - N_{I,\text{add}} / \langle \hat{I}_I^2 \rangle, \quad (32)$$

$$\xi = G_I / 2 \langle \hat{I}_I^2 \rangle. \quad (33)$$

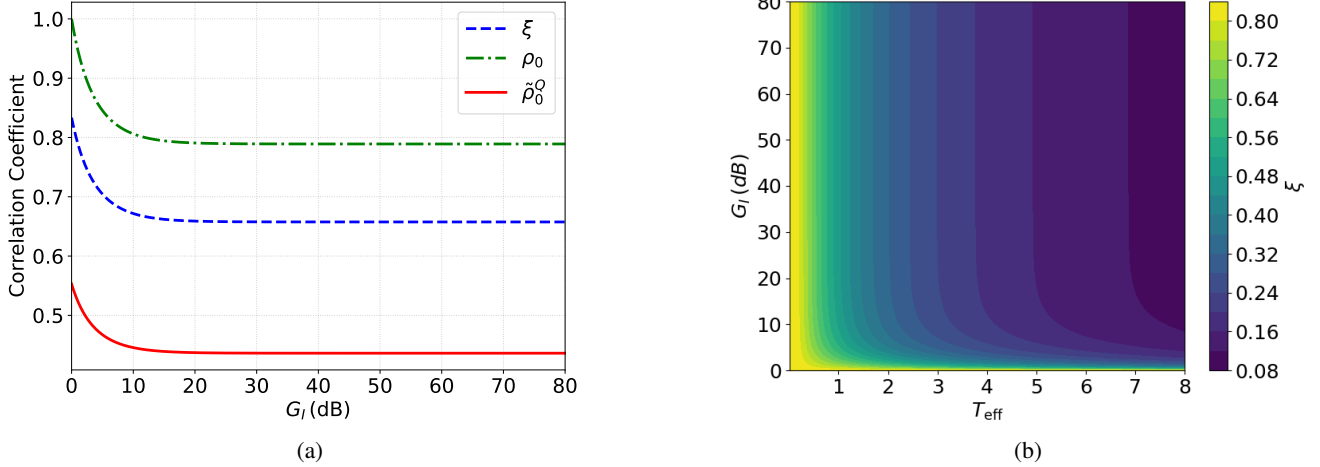


FIG. 4: (Color online) (a) The modified correlation coefficient  $\tilde{\rho}_0$ , the correlation coefficient  $\tilde{\rho}_0$  reported in Ref<sup>35</sup>, and the correction term  $\xi$  versus the amplification gain of the idler mode  $G_I$ . The noise figure and the effective temperature of the idler amplifier are fixed at  $\text{NF} = 1$  dB and  $T_{\text{eff}} = 500$  mK, respectively. (b) The correction term  $\xi$  as the function of the idler amplifier temperature  $T_{\text{eff}}$  and gain  $G_I$  for the noise figure of  $\text{NF} = 1$  dB. In both figures, the photon number per mode is set to  $N_s = 0.1$ .

Equation (30) is the range equation for the quantum-entangled noise radar, which enables us to evaluate the residual Pearson correlation coefficient between the returned signal (from the target at a range  $R$ ) and idler modes.

It is important to highlight that Eq. (30) represents the modified version of the expression introduced in Ref<sup>35</sup>. It contains an additional correction term,  $\xi^2$ , which depends on the amplifier gain, the added noise, and the average photon number per mode. This correction term is generally non-negligible and results in a reduction of the correlation coefficient compared to the value reported in Ref. <sup>35</sup>. To show this, we have illustrated the behavior of the modified Pearson correlation coefficient  $\tilde{\rho}_0^{\text{QI}}$ , the correction term  $\xi$ , and the original correlation coefficient  $\rho_0$  versus the idler amplification gain  $G_I$  in Figure 4a for  $N_s = 0.1$ ,  $\text{NF} = 1$  dB, and  $T_{\text{eff}} = 500$  mK. As shown in this figure, for the parameters considered here, the modified correlation coefficient is approximately 44.72% lower than the coefficient  $\rho_0$ . This that the contribution of the amplifier noise must be included in the Pearson correlation coefficient. From Eq. (31), it is evident that the modified correlation coefficient  $\tilde{\rho}_0^{\text{QI}}$  approaches  $\rho_0$  in the limit of  $\xi \rightarrow 0$ . According to Eq. (33), in the regime where  $N_s \ll 1$ , in which the QI protocol outperforms the best classical strategies, this limit is satisfied when  $N_I^{\text{amp}} \gg 1$ . On the other hand, the condition  $N_I^{\text{amp}} \gg 1$  is, in turn, satisfied when the idler amplifier operates at high temperatures. This behavior is further demonstrated in Fig. 4b, where the correction term  $\xi$  is plotted versus the idler amplification gain  $G_I$  and the effective temperature  $T_{\text{eff}}$ . As is evident, the correction term is significantly influenced by the effective temperature, while its variation with respect to  $G_I$  is relatively modest. Specifically, the correction term drops below 0.16 for  $T_{\text{eff}} > 5$  K. In quantum-entangled noise radars, due to the fragility of quantum correlations to noise, it is beneficial to employ low-noise amplifiers operating at cryogenic tempera-

tures, for which  $N_I^{\text{amp}}$  is small<sup>31,59</sup>. Under this condition, the correction term becomes substantial, and hence,  $\tilde{\rho}_0^{\text{QI}} < \rho_0$ .

If detection occurs by integrating over  $M = \tau_{\text{int}} B_{\text{det}}$  samples, in which  $\tau_{\text{int}}$  is the integration time and  $B_{\text{det}}$  is the detection bandwidth, the SNR of the received signal and idler modes increases by the factor  $M$ . Therefore, the effective correlation coefficient becomes

$$\rho_{\text{QI}}^{\text{eff}}(R) \simeq \frac{\tilde{\rho}_0^{\text{QI}}}{\sqrt{1 + \frac{1}{M G_{\text{S,rec}} F^2(R)} \left(\frac{R}{R_c}\right)^4}}, \quad (34)$$

where  $R_c$  represents the characteristic range of the quantum-entangled noise radar, and is given by

$$R_c = \left( \frac{\sigma_{GA_e} \langle \hat{I}_I^2 \rangle_{\text{QI}}}{(4\pi)^2 N_n} \right)^{1/4}. \quad (35)$$

In Fig. 5, we have shown how key system parameters, such as the signal-idler amplification gains, integration time  $\tau_{\text{int}}$ , and signal bandwidth  $B_{\text{sig}}$ , affect the normalized Pearson correlation coefficient,  $\rho_{\text{QI}}^{\text{eff}}/\tilde{\rho}_0^{\text{QI}}$ . As shown in Fig. 5a, increasing the signal gain at the receiver,  $G_{\text{S,rec}}$ , has a negligible impact on the correlation coefficient, while increasing the idler gain,  $G_I$ , significantly enhances it. This is due to the fact that the term  $N_n/(G_{\text{S,rec}} \langle \hat{I}_I^2 \rangle)$  that appeared in Eq. (30) remains nearly independent of  $G_{\text{S,rec}}$ , but it is scaled inversely with  $G_I$ . Moreover, Fig. 5b shows that increasing either  $\tau_{\text{int}}$  or  $B_{\text{sig}}$  enhances the correlation between the detected signal and idler fields. Increasing both the signal bandwidth and the integration time raises the effective signal power, thereby improving the SNR at the receiver. Note that increasing  $B_{\text{sig}}$  directly decreases the photon number per mode,  $N_s$ .

In quantum-entangled noise radars, the presence of the target is declared when the effective correlation coefficient exceeds

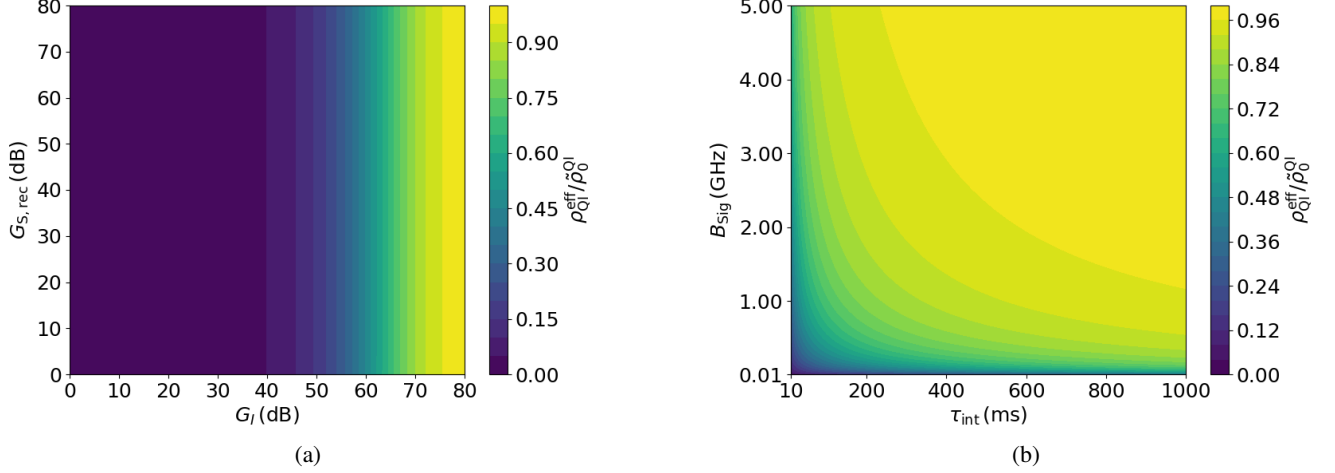


FIG. 5: (Color online) The normalized Pearson correlation coefficient  $\rho_Q^{\text{eff}}/\rho_0^Q$  versus (a) amplification gain of the idler mode  $G_I$  and gain of the signal mode at the receiver  $G_{S,\text{rec}}$  for the target at range of  $R = 1$  km, and (b) the integration time  $\tau_{\text{int}}$  and the bandwidth of the signal mode  $B_{\text{sig}}$  for  $G_I = G_{S,\text{rec}} = 80$  dB. In both cases, the noise figure and effective temperature of the idler and signal amplifiers are fixed at  $\text{NF} = 1$  dB and  $T_{\text{eff}} = 100$  mK, respectively. Moreover, the target range is considered to be  $R = 1$  km, and the photon number per mode is set to  $N_s = 0.1$ . Other system parameters are the same as in Fig. 2.

a threshold value,  $\rho_{\text{th}}$ . This leads to  $\rho_{\text{QI}}^{\text{eff}}(R) \geq \rho_{\text{th}}$ , which is referred to as the detection condition for noise radars. Note that the threshold correlation coefficient,  $\rho_{\text{th}}$ , depends on the number of integration samples  $M$  and the false alarm probability  $P_{\text{fa}}$  for the target detection, which is determined by  $\rho_{\text{th}} = \sqrt{-\ln P_{\text{fa}}/M}$ <sup>60</sup>. By substituting the effective correlation coefficient obtained in Eq. (34) into the detection condition, and considering that the equality holds for the maximum detection range, we obtain

$$R_{\text{max}} \times 10^{\frac{\gamma R_{\text{max}}}{20}} = M^{\frac{1}{4}} \left[ \left( \frac{\tilde{\rho}_0^{\text{QI}}}{\rho_{\text{th}}} \right)^2 - 1 \right]^{\frac{1}{4}} R_c. \quad (36)$$

By comparing this expression with its counterpart for the direct detection radars obtained in Eq. (3), we found that the term  $[(\tilde{\rho}_0^{\text{QI}}/\rho_{\text{th}})^2 - 1]^{1/4}$  on the right-hand side of Eq. (36) analogously plays the role of the term  $(\text{SNR}_{\text{th}})^{-1/4}$  which is appeared on the right-hand side of Eq. (3) for direct detection radars. This analogy motivates us to define an effective threshold SNR for the target detection in quantum-entangled noise radars as

$$\text{SNR}_{\text{th,eff}}^{\text{QI}} \equiv \left[ \left( \frac{\tilde{\rho}_0^{\text{QI}}}{\rho_{\text{th}}} \right)^2 - 1 \right]^{-1}. \quad (37)$$

This definition allows us to interpret the quantum-entangled noise radar as a direct detection radar with the effective threshold SNR that obtained by Eq.(37).

In Fig. 6, we have shown the influence of different parameters of the system, such as the integration time  $\tau_{\text{int}}$ , false-alarm probability  $P_{\text{fa}}$ , and mean signal-idler photon number per mode

$N_s$  on the effective threshold SNR of quantum-entangled noise radars (Eq. (37)). As shown in Fig. 6, the effective threshold SNR for target detection in quantum-entangled noise radars is significantly lower than that of classical direct-detection radars, which are typically greater than 10 dB<sup>8</sup>. As discussed earlier in Sec. II, the maximum detection range of a direct-detection radar increases as the threshold SNR decreases. Since a quantum-entangled noise radar effectively behaves as a direct-detection radar with a reduced threshold SNR, we expect its maximum detection range to exceed that of analogous classical direct-detection radars with the same system parameters. Figure 6a demonstrates that  $\text{SNR}_{\text{th,eff}}^{\text{QI}}$  decreases with increasing  $\tau_{\text{int}}$  and  $P_{\text{fa}}$ . Moreover, Figure 6b shows that increasing  $N_s$  leads to a reduction of the effective threshold SNR for target detection.

By substituting Eq. (37) into Eq. (36), and solving the resulting equation for  $R_{\text{max}}$ , one can obtain the maximum detection range of the quantum-entangled noise radar in terms of the Lambert W function as follows

$$R_{\text{max}}^{\text{QI}} = \frac{20}{\ln(10)\gamma} W_0 \left[ \frac{\ln(10)}{20} \gamma \left( \frac{M}{\text{SNR}_{\text{th}}^{\text{QI}}} \right)^{1/4} R_c \right]. \quad (38)$$

This equation allows us to evaluate the performance of a quantum-entangled noise radar by considering the system, environment, and target parameters. In the next subsection, we will calculate the analogous relation for classical-correlated noise radars to compare their performance under the same operational conditions.

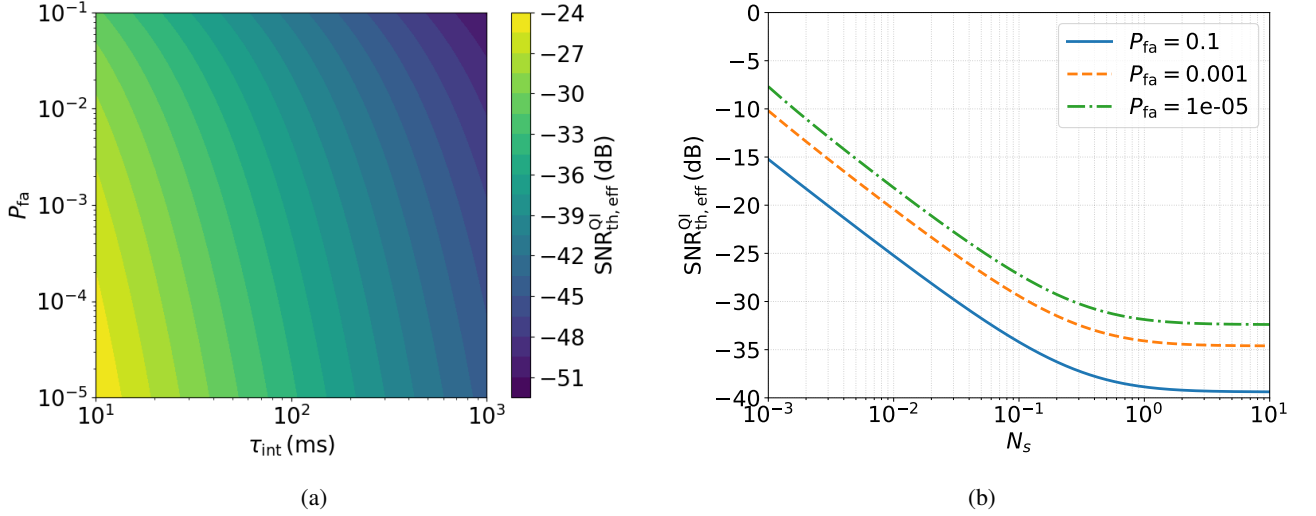


FIG. 6: (Color online) The effective threshold SNR for the quantum entangled noise radars  $\text{SNR}_{\text{th,eff}}^{\text{QI}}$  in term of (a) the false-alarm probability of the target detection  $P_{\text{fa}}$  and the integration time  $\tau_{\text{int}}$  for fixed value  $N_s = 0.1$ , and (b) the mean photon number per mode  $N_s$  for  $\tau_{\text{int}} = 100$  ms and different values of the false-alarm probability as  $P_{\text{fa}} = \{10^{-1}, 10^{-3}, 10^{-5}\}$ . The other system parameters considered here are the same as in Fig. 5.

### B. Maximum Detection Range of Classical-Correlated Noise Radars

In an ideal classical-correlated noise radar, the correlated signal and idler fields are produced by splitting a coherent state of a microwave field by means of a power divider or beam splitter. A power divider is characterized by its complex transmission  $t$  and reflection  $r$  coefficients (satisfying  $|t|^2 + |r|^2 = 1$ ), and the relative phase  $\varphi$  between the transmission and reflection paths. The two input fields that incident on the input ports of the power divider described by the annihilation operators  $\hat{a}_1$  and  $\hat{a}_2$ . The output field operators of the power divider, i.e., the signal and idler ports, denoted by  $\hat{a}_S$  and  $\hat{a}_I$ , respectively, are related to the input operators via the following transformation<sup>61</sup>

$$\begin{pmatrix} \hat{a}_S \\ \hat{a}_I \end{pmatrix} = \begin{pmatrix} |t| & e^{i\varphi}|r| \\ -e^{-i\varphi}|r| & |t| \end{pmatrix} \begin{pmatrix} \hat{a}_1 \\ \hat{a}_2 \end{pmatrix}. \quad (39)$$

This relation describes the coherent mixing of the input modes and determines the quantum state of the output fields.

Suppose that the quantum state of the input port 1 being the coherent state  $|\alpha\rangle$  with  $\alpha = |\alpha|e^{i\theta}$ , and the input port 2 being the vacuum state  $|0\rangle$ . Thus, the joint quantum state of the input fields is given by  $|\Psi\rangle_{\text{in}} = |\alpha\rangle_1 \otimes |0\rangle_2$ . Analogous to the quantum scheme, we should calculate the Pearson correlation coefficient that previously defined in Eq. (13) to evaluate the correlation between these fields. By assuming an ideal balanced power divider, i.e.  $|t|^2 = |r|^2 = 1/2$ , and  $\varphi = \pi$  ( $\pi$  radians phase shift during reflection), considering the phase of the coherent state as  $\theta = 0$  without the loss of generality, and

also using the joint quantum state  $|\Psi\rangle_{\text{in}}$ , we get to

$$\langle \hat{I}_S^2 \rangle_{\text{CI}} \simeq \eta(R)G_S(|\alpha|^2 + \frac{1}{2}) + N_{S,\text{add}}^{(1)}, \quad (40)$$

$$\langle \hat{I}_I^2 \rangle_{\text{CI}} \simeq G_I(|\alpha|^2 + \frac{1}{2}) + N_{I,\text{add}}, \quad (41)$$

$$\langle \hat{I}_S \hat{I}_I \rangle_{\text{CI}} = \sqrt{\eta(R)G_S G_I} |\alpha|^2. \quad (42)$$

By considering that  $|\alpha|^2 = N_s$  in order to have an analogy between the classical and quantum cases, one finds  $\langle \hat{I}_S^2 \rangle_{\text{CI}} = \langle \hat{I}_S^2 \rangle_{\text{QI}}$  and  $\langle \hat{I}_I^2 \rangle_{\text{CI}} = \langle \hat{I}_I^2 \rangle_{\text{QI}}$ , while  $\langle \hat{I}_S \hat{I}_I \rangle_{\text{QI}} = Q_{\text{adv}} \times \langle \hat{I}_S \hat{I}_I \rangle_{\text{CI}}$  where

$$Q_{\text{adv}} = \sqrt{1 + \frac{1}{N_s}}, \quad (43)$$

denotes the quantum advantage. By noticing Eq. (13) one can conclude that the Pearson correlation coefficient for the quantum-entangled fields is  $Q_{\text{adv}}$  times greater than the classically correlated ones. Therefore, the Pearson correlation coefficient for the classically correlated fields can be written as

$$\rho_{\text{CI}}^{\text{eff}}(R) \simeq \frac{\tilde{\rho}_0^{\text{CI}}}{\sqrt{1 + \frac{1}{MG_{S,\text{rec}}F^2(R)} \left(\frac{R}{R_c}\right)^4}}, \quad (44)$$

where  $\tilde{\rho}_0^{\text{CI}} = \tilde{\rho}_0^{\text{QI}}/Q_{\text{adv}}$  is the Pearson correlation coefficient of the classical correlated fields. Equation (44) shows that under the identical conditions, the correlation between the two quantum-entangled signal-idler fields prepared in the TMSV state is enhanced by the factor of  $Q_{\text{adv}}$  compared to the ideal classical-correlated fields. It should be noted that the quantum advantage appeared here originates from the quantum entanglement, which never has the classical counterpart.

By applying the detection condition analogous to the quantum-entangled noise radar, we have derived an explicit

expression for the maximum detection range of the classical-correlated noise radar as follows

$$R_{\max}^{\text{CI}} = \frac{20}{\ln(10)\gamma} W_0 \left[ \frac{\ln(10)}{20} \gamma \left( \frac{M}{\text{SNR}_{\text{th}}^{\text{CI}}} \right)^{1/4} R_c \right], \quad (45)$$

where  $\text{SNR}_{\text{th}}^{\text{CI}}$  denotes the effective threshold SNR for the classical illumination target detection, and is given by

$$\text{SNR}_{\text{th}}^{\text{CI}} = \left[ \left( \frac{\tilde{\rho}_0^{\text{CI}}}{\rho_{\text{th}}} \right)^2 - 1 \right]^{-1}. \quad (46)$$

We are now going to compare the maximum detection ranges of a classical-correlated noise radar and a quantum-entangled noise radar with identical system parameters in the following subsection.

### C. Range Enhancement Factor

In order to gain insight into the performance of quantum-entangled noise radars, it is beneficial to compare their maximum detection range with that of classical ones under identical operational conditions. To this end, we have defined the parameter *range enhancement factor* (REF) as the ratio of the maximum detection range of a quantum-entangled noise radar to that of a classically correlated one, i.e.,  $\text{REF} \equiv R_{\max}^{\text{QI}}/R_{\max}^{\text{CI}}$ , for identical system parameters. From Eqs. (38) and (45), the REF can be obtained as follows

$$\text{REF} = \frac{W_0 \left[ \frac{\ln(10)}{20} \gamma \left( \frac{M}{\text{SNR}_{\text{th}}^{\text{QI}}} \right)^{1/4} R_c \right]}{W_0 \left[ \frac{\ln(10)}{20} \gamma \left( \frac{M}{\text{SNR}_{\text{th}}^{\text{CI}}} \right)^{1/4} R_c \right]}. \quad (47)$$

However, since  $W_0(x) = \sum_{n=1}^{\infty} (-1)^{n-1} x^n / n!$ <sup>41</sup>, for  $\gamma \ll 1$  one can approximate the the Lambert W-function  $W_0$  in Eq. (47) by  $W_0(x) \approx x$ . Therefore, for  $\gamma \ll 1$  one can conclude that

$$\text{REF} \approx \left( \frac{\text{SNR}_{\text{th}}^{\text{CI}}}{\text{SNR}_{\text{th}}^{\text{QI}}} \right)^{1/4}. \quad (48)$$

On the other hand, from Eqs. (37) and (46), one can show, after some straightforward calculations, that

$$\frac{\text{SNR}_{\text{th}}^{\text{QI}}}{\text{SNR}_{\text{th}}^{\text{CI}}} \propto \begin{cases} 1 & N_s \gg 1 \\ 1/Q_{\text{adv}}^2 & N_s \ll 1 \end{cases}. \quad (49)$$

Therefore, in the limit of  $\gamma \ll 1$ , the range enhancement factor can be approximated by

$$\text{REF} \approx \sqrt{Q_{\text{adv}}}. \quad (50)$$

This relation provides a straightforward tool for comparing the maximum detection range of quantum-entangled noise radars with their classical counterparts.

The difference between the exact analytical expression for REF obtained in Eq. (47) and its approximate value in Eq. (50) is quantified by

$$\delta = \frac{\text{REF} - \sqrt{Q_{\text{adv}}}}{\sqrt{Q_{\text{adv}}}}. \quad (51)$$

In order to examine the validity of the approximations that were introduced previously, we have plotted the exact analytical value of the REF obtained in Eq. (47) and its approximate value in Eq. (50), with respect to  $N_s$  in Fig. 7a. This plot shows that there is good agreement between the exact value of the REF and its approximation obtained in Eq. (50). In this figure, the difference  $\delta$  is displayed for some values of the mean photon number per mode, as  $N_s = 10^{-3}, 10^{-2}, 10^{-1}, 1$ . It is evident that the difference is just 0.0888 for  $N_s = 10^{-3}$ , and it is reduced to less than 0.0004 for larger values of  $N_s$ . Figure 7b gives more insight into the variation of  $\delta$  in terms of  $N_s$ . It shows that the difference between the exact and approximate values of the REF is about 8.9% for  $N_s = 10^{-3}$ , and it gradually vanishes as  $N_s$  increases. This demonstrates that Eq. (50) gives a good approximation for the REF.

Let us now discuss the REF from the engineering point of view. As demonstrated previously in Eq. (48), for  $\gamma \ll 1$ , one can approximate the REF as the fourth root of the ratio between the threshold SNR of a classical-correlated noise radar and that of a quantum-entangled one. It is straightforward to rewrite this equation as follows

$$\text{REF} \approx 2^{\Delta\text{SNR}_{\text{th}}^{(\text{dB})}/12}, \quad (52)$$

where  $\Delta\text{SNR}_{\text{th}}^{(\text{dB})} \equiv \text{SNR}_{\text{th}}^{\text{CI}(\text{dB})} - \text{SNR}_{\text{th}}^{\text{QI}(\text{dB})}$ . According to this equation, which makes practical sense, each 12dB reduction in the threshold SNR by means of the quantum entanglement doubles the REF. From Eqs. (50), (52), and (43), it is straightforward to show that for  $N_s \ll 1$  (which is the case of quantum illumination), the parameter  $\Delta\text{SNR}_{\text{th}}^{(\text{dB})}$  can be approximated as

$$\Delta\text{SNR}_{\text{th}}^{(\text{dB})} \approx -3 \log_2(N_s), \quad (53)$$

In conclusion, Eqs (47), (50), (52), and (53) provide a practical tool from the engineering point of view to compare the performance of the quantum and classical versions of noise radars. As an example, for  $N_s \simeq 0.25$ , we have  $\Delta\text{SNR}_{\text{th}}^{(\text{dB})} = 6$  dB, which results in  $\text{REF} \simeq 1.41$ , i.e., about 40% superiority of the maximum detection range of the quantum-entangled noise radar over the classical-correlated one with the same operational conditions.

### D. Results

Previously, we developed the analytical framework for evaluating the maximum detection range of quantum-entangled noise radars, as well as their classical counterparts. This framework allows us to investigate whether a quantum-entangled noise radar is capable of detecting targets at long ranges in the

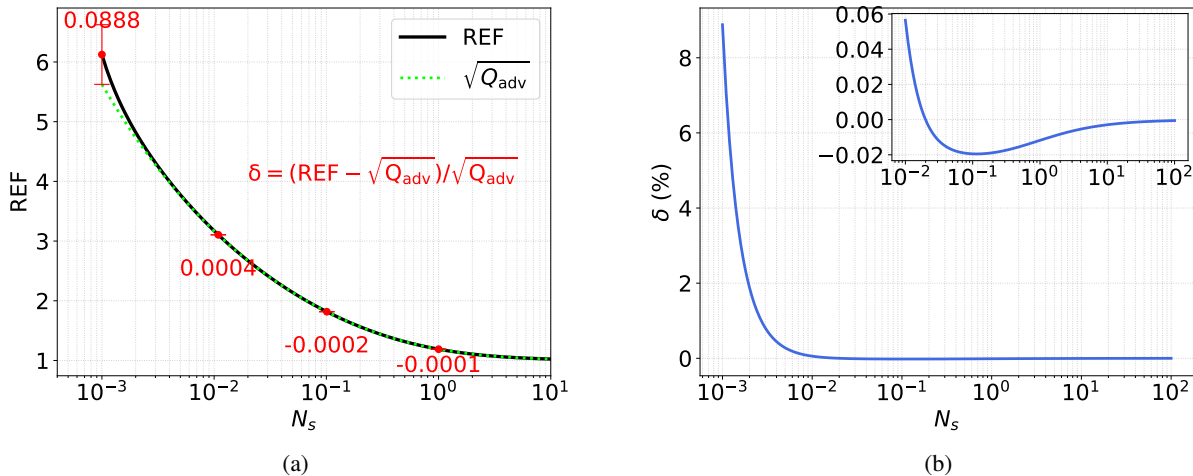


FIG. 7: (Color online) (a) The range enhancement factor, REF, versus the photon number per mode,  $N_s$ , based on the analytical expression obtained in Eq. (47) (solid-black line) and the approximation result given in Eq. (50) (dotted-green line). The difference  $\delta$  is shown with the vertical red error bars for  $N_s = 10^{-3}, 10^{-2}, 10^{-1},$  and  $1$ . (b) The difference between the exact analytical and approximate expressions for REF, i.e.,  $\delta$  vs  $N_s$ . The other system parameters considered here are  $f_s = f_i = 9$  GHz,  $B_{\text{sig}} = 500$  MHz.

order of several kilometers. More specifically, it allows us to examine the conditions under which such detection might be achievable. To address this issue, we assessed the maximum detection range of these systems using a set of realistic parameters based on current technological capabilities, as summarized in Table II. It is important to note that we do not claim any experimental realization of a quantum-entangled radar system operating with the parameters outlined in Table II.

TABLE II: The system parameters considered for a quantum-entangled noise radar.

Parameter	Value	Unit
Microwave Photon Pair Source	JTWPA	-
$f_s$	9	GHz
$f_i$	9	GHz
$B_{\text{sig}}$	8	GHz
$G_{\text{tr}}$	80	dB
$G_{\text{S,rec}}$	20	dB
$T_{\text{amp}}$	10	mK
NF	1	dB
$T_{\text{env}}$	300	K
$\tau_{\text{int}}$	200	ms
$B_{\text{det}}$	50	MHz
$N_s$	0.05	-
$\epsilon_a$	0.9	-
$A$	$\pi$	$\text{m}^2$
$P_{\text{fa}}$ (search mode)	$10^{-1}$	-
$P_{\text{fa}}$ (track mode)	$10^{-3}$	-

Following the approach outlined in Ref. <sup>62,63</sup>, we consider a quantum-entangled noise radar utilizing a state-of-the-art

flux-driven Josephson traveling-wave parametric amplifier (JTWPA) as the source of entangled microwave-photon pairs. This device is capable of emitting degenerate signal and idler fields at frequencies  $f_s = f_i = 9$  GHz, with an average photon number per mode of  $N_s = 0.05$ , and a 3-dB bandwidth at the signal center frequency. This performance arises from the efficient three-wave mixing and broadband phase matching, which are enabled by the circuit's nonlinear dispersion and the separate pump-signal configuration<sup>63</sup>. Consequently, the signal bandwidth of  $B_{\text{sig}} = 8$  GHz considered in Table II is experimentally achievable with this technology. The total transmitter gain is assumed to be 80 dB, which is consistent with that reported in Ref.<sup>31</sup>. Additionally, the signal amplification gain at the receiver is considered to be  $G_{\text{S,rec}} = 20$  dB. We assumed the detection time as 200 ms, which is appropriate for detecting medium-sized objects at velocities of approximately 20 – 30 m/s over distances up to 1 km<sup>64</sup>. This is justified by the fact that the object's displacement during the detection interval is less than 0.60% of its range, ensuring minimal impact of target movement on the detection.

Two operational modes based on the target detection false-alarm probability are considered: track mode ( $P_{\text{fa}} < 0.01$ ) and search mode ( $0.01 < P_{\text{fa}} < 0.5$ ). According to Eq. (38), the quantum-entangled noise radar with the parameters listed in Table II is capable of detecting an object with an RCS of  $\sigma = 0.1 \text{ m}^2$  at a maximum range of  $R_{\text{max}} = 1.56$  km in the search mode ( $P_{\text{fa}} = 0.1$ ) and  $R_{\text{max}} = 1.19$  km in the track mode ( $P_{\text{fa}} = 0.001$ ).

It is important to emphasize that, for  $N_s = 0.05$ , the considered system shows  $\text{REF} \simeq 2.14$ ,  $Q_{\text{adv}} \simeq 4.58$ , and  $\Delta\text{SNR}_{\text{th}}^{(\text{dB})} = 13.18$  dB. This refers to the fact that, by utilizing entanglement, the maximum detection range of the considered system exceeds by a factor of 2.14, and the threshold SNR is reduced

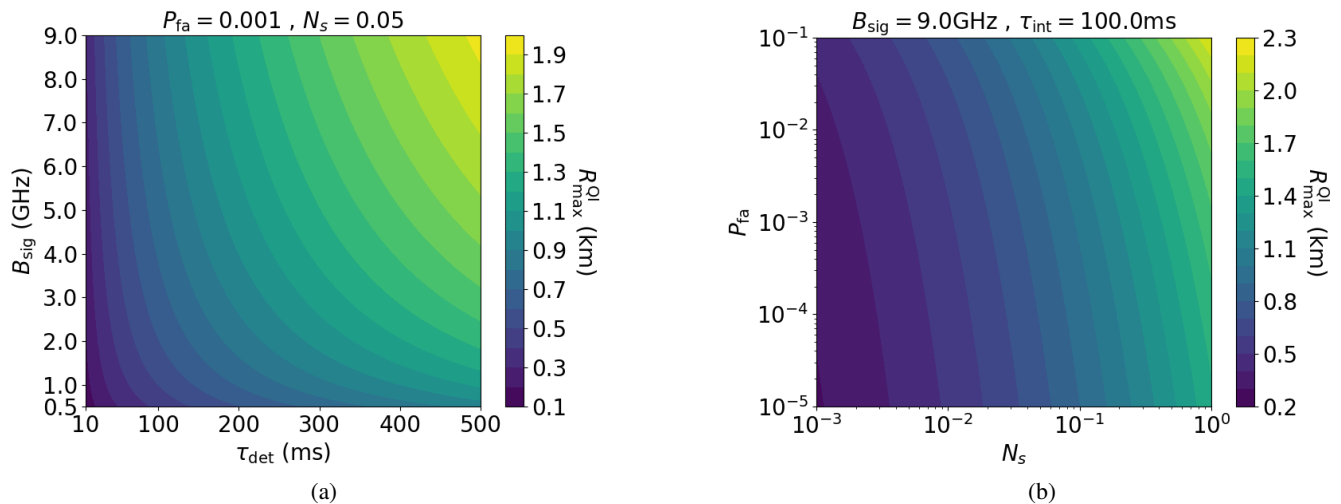


FIG. 8: (Color online) The maximum detection range of the quantum-entangled noise radar,  $R_{\max}^{\text{QI}}$ , in terms of: (a) the detection time  $\tau_{\text{int}}$  and the signal bandwidth  $B_{\text{sig}}$  for  $P_{\text{fa}} = 10^{-3}$  and  $N_s = 0.05$  (corresponding to REF = 2.14), and (b) the mean photon number per mode  $N_s$  and the false-alarm probability  $P_{\text{fa}}$  for  $B_{\text{sig}} = 9$  GHz and  $\tau_{\text{int}} = 50$  ms. The other system parameters are the same as given in Table II.

by 13.18 dB, compare to its analogous classical-correlated noise radar under the same operational conditions. Moreover, it shows that the signal and idler modes in the considered quantum-entangled noise radar have a correlation which is 4.54 times stronger than the classical case.

To provide further insight, we analyze the impact of the key system parameters on the maximum detection range of the considered quantum-entangled noise radar in Fig. 8. Figure 8a shows the influence of the integration time  $\tau_{\text{int}}$  and the signal bandwidth  $B_{\text{sig}}$  on the maximum detection range of the quantum-entangled noise radar with parameters listed in Table II in the track mode with  $P_{\text{fa}} = 0.001$ . It also demonstrates that with an ultra-wideband signal with  $B_{\text{sig}} \sim 9$  GHz and a sufficiently long detection time as  $\tau_{\text{int}} = 500$  ms, tracking low reflective objects with  $\sigma = 0.1$  m<sup>2</sup> up to 2 km is possible with the considered system. Moreover, it shows the importance of the signal bandwidth on the maximum detection range of the quantum-entangled noise radar. As an example, for the given integration time as  $\tau_{\text{int}} = 100$  ms, the maximum detection range increases from 420 m to 866 m when the signal bandwidth rises from 500 MHz to 9 GHz. The effect of the false-alarm probability,  $P_{\text{fa}}$ , and the mean photon number of the generated signal and idler fields per mode,  $N_s$ , on the maximum detection range is demonstrated in Fig. 8b. In this figure, we have considered a signal with ultra-high bandwidth of  $B_{\text{sig}} = 9$  GHz and a relatively short integration time as  $\tau_{\text{int}} = 100$  ms. As is seen, for  $N_s = 1$  (corresponding to  $Q_{\text{adv}} = 1.41$  and REF  $\simeq 1.18$ ), the maximum detection range reaches 2.2 km and 1.67 km in the search and track modes, respectively. However, for a low value of the photon number per mode as  $N_s = 0.01$  where the quantum advantage and REF are substantial, the maximum detection range reaches to 769 m in the search mode and 584 m in the track mode.

It is important to note that the parameters proposed in Ta-

ble II are practically achievable with the current state-of-the-art technology. To support this claim, we compare these parameters with those of the previously implemented quantum-entangled noise radars, as summarized in Table III. This table presents the key system parameters of three notable quantum radar implementations which are reported to date<sup>31,59,65</sup>, to the best of our knowledge. In order to estimate the maximum detection range of these systems, we consider a transmission antenna characterized by the gain of  $G = 15$  dB, the aperture efficiency of  $\epsilon_a = 0.9$ , and the radius  $r = 1$  m. The target is assumed to be a small object with the RCS of  $\sigma = 0.1$  m<sup>2</sup>. The false-alarm probability is set to  $P_{\text{fa}} = 0.1$  for the search mode and  $P_{\text{fa}} = 0.001$  for the track mode. The atmospheric absorption coefficient of  $\gamma = 0.007$  dB/km is also considered. Under these conditions, the maximum detection range of the quantum-entangled noise radar reported in<sup>59</sup> is estimated to be 17.82 m in the search mode. For the system described in<sup>31</sup>, the estimated range increases to 378.6 m, while the radar reported in<sup>65</sup> achieves the maximum range of 354.42 m. In the track mode, the corresponding maximum detection ranges are estimated as 13.54 m for<sup>59</sup>, 285.75 m for<sup>31</sup>, and 269 m for<sup>65</sup>.

As shown in Table III, the system presented in Ref.<sup>65</sup> has the highest quantum advantage,  $Q_{\text{adv}}$ , among the three. This enhanced performance is primarily attributed to the lower signal photon number  $N_s$  utilized in the system. While the radar demonstrated in<sup>59</sup> yields the lowest performance in terms of both maximum detection range and quantum advantage, it offers a notably short integration time, making it more aligned with real-time field applications. Furthermore, the longer detection range of the system in Ref.<sup>65</sup> is due to its high signal bandwidth. In addition, it could be further improved through the use of a higher-gain amplifier at the transmitter, as well as by increasing the transmitted signal photon number per mode  $N_s$ .

TABLE III: List of the system parameters for some representative quantum-entangled radars implemented to-date (based to our knowledge). JPC: Josephson Parametric Converter; JPA: Josephson Parametric Amplifier; JTWPA: Josephson Traveling Wave Parametric Amplifier.

Parameter	Unit	Ref. <sup>31</sup>	Ref. <sup>59</sup>	Ref. <sup>65</sup>
Source	-	JPC	JPA	JTWPA
$f_S$	GHz	10.09	7.5376	3.3
$f_i$	GHz	6.8	6.1445	3.45
$B_{\text{sig}}$	MHz	20	1	3,000
$G_{\text{tr}}$	dB	77.16	63	30
$N_b$	-	672	1015	100
$\tau_{\text{int}}$	ms	1,900	50	-
$B_{\text{det}}$	kHz	200	1,000	-
$M$	-	$3.8 \times 10^5$	$5 \times 10^4$	$1.5 \times 10^7$
$N_s$	-	0.5	0.57	0.05
$Q_{\text{adv}}$	-	1.73	1.65	4.58
REF	-	1.32	1.29	2.14

It is worthwhile to note that the objective of this study is to evaluate the ultimate performance of quantum-entangled noise radars. For this purpose, up to now we have assumed that the receiver antenna is ideal, capable of detecting any weak signal incident upon it. In reality, however, various microwave detection technologies have limitations in detecting weak signals, which may have an impact on the performance of the radar system. This issue will be addressed in the subsequent subsection III E.

## E. Challenges and Limitations

Thus far, we have comprehensively examined the practical aspects of quantum-entangled noise radars. We have also investigated the feasibility of implementing such systems with a maximum detection range in the order of few kilometers. However, several operational challenges remain, as identified by the quantum radar community, which we are going to address in the following.

### 1. Power of the Received Signal

One important concern regarding the operation of quantum-entangled noise radars is whether the power of the signal back-scattered from the target and reaches the radar receiver is sufficient to be detected. The radar receiver antenna can detect any signal whose power exceeds a fundamental physical detection limit (PDL). It is defined as the minimum incident electromagnetic power required to induce a measurable electrical current or voltage at the antenna terminals. This limit is fundamentally determined by the antenna's material properties, geometry, and quantum effects, and is independent of the receiver system or signal processing techniques.

For microwave antennas, the PDL corresponds to the power level at which the conduction current induced by the incident

wave becomes comparable to the intrinsic thermal agitation of electrons within the antenna structure. This establishes a bound below which no physical signal can be observed<sup>8</sup>.

It is important to distinguish the PDL from both the antenna noise floor and the MDS defined in Eq. (7). The noise floor refers to the total noise power present at the receiver input, which includes thermal noise contributions from the antenna and front-end electronics. Therefore, it defines the practical sensitivity threshold for signal detection. MDS is a higher threshold that incorporates the system noise figure and the required SNR for achieving the specified detection and false alarm probabilities. In contrast to the noise floor and MDS, the PDL is an intrinsic property of the antenna and cannot be reduced through improvements in the receiver design or the signal processing.

It should be emphasized that in certain radar systems, such as noise radars (either classical or quantum) or those employing coherent processing and pulse coded or shaped waveforms, thanks to the processing gain, signals below the noise floor can be detected using advanced techniques such as integration, correlation, or matched filtering. However, such processing gains are ultimately constrained by the PDL of the antenna or detector. If the incident signal power is below this fundamental threshold, then it fails to induce any measurable electrical response. Therefore, it is trivial that no signal processing technique can recover it, as the signal does not physically exist in the received output.

Unlike the noise floor and MDS, the PDL of an antenna is not typically expressed by a simple universal formula. However, an approximate physical interpretation can be obtained by modeling the antenna as a resistor at temperature  $T_a$ , characterized by a Johnson-Nyquist noise current which is given by<sup>70</sup>

$$i_n = \sqrt{\frac{4k_B T_a B_a}{R_a}}. \quad (54)$$

Here,  $i_n$  is the root mean square (RMS) noise current,  $B_a$  is the antenna bandwidth, and  $R_a$  is the antenna radiation resistance. If a signal with the power  $P$  incidents on an antenna, then the induced signal current is determined by

$$i_s = \sqrt{\frac{P}{R_a}}. \quad (55)$$

The PDL corresponds to the minimum signal power for which the induced signal current,  $i_s$ , exceeds the noise current,  $i_n$ . Therefore, by utilizing Eqs. (54) and (55), one can obtain the PDL of classical antennas as follows

$$P_{\text{PDL}}^{\text{CA}} \approx 4k_B T_a B_a. \quad (56)$$

For instance, a high-performance antenna with an effective noise temperature of  $T_a = 30$  K and a bandwidth of  $B_a = 50$  MHz exhibits a PDL of  $P_{\text{PDL}}^{\text{CA}} = 8.3 \times 10^{-14}$  W ( $-100.8$  dBm). In contrast, a commercial antenna operating at  $T_a = 290$  K with the same bandwidth has a PDL of  $P_{\text{PDL}}^{\text{CA}} = 8.0 \times 10^{-13}$  W ( $-90.97$  dBm).

In the case of SMPDs, the PDL can be estimated based on the detector's DCR. In this case, the detector's PDL is

limited by the DCR-equivalent power. By considering the quantum efficiency of the SMPD as  $\eta_Q^{\text{SMPD}}$ , the PDL can be approximated as

$$P_{\text{PDL}}^{\text{SMPD}} \approx \frac{1}{\eta_Q^{\text{SMPD}}} h f_s \times \text{DCR}_{\text{SMPD}}, \quad (57)$$

where  $f_s$  is the signal frequency. According to this relation, the PDL for the SMPD reported in Ref.<sup>42</sup> with a DCR of 30 Hz and the quantum efficiency of  $\eta_Q^{\text{SMPD}} = 0.8$  can be found as  $P_{\text{PDL}}^{\text{SMPD}} \approx 2.12 \times 10^{-22}$  W (−186.55 dBm).

Another solution for detecting extremely weak microwave signals efficiently and preserving its quantum state simultaneously, is based on quantum microwave-to-optical transducers, as denoted in Ref.<sup>71</sup>. In this method, the weak microwave signal arrives at the radar receiver should be coherently converted to the optical domain using a quantum microwave-to-optical transducer, and subsequently, the optical signal is detected by utilizing a high quantum-efficiency SOPD. Quantum transducers with high conversion efficiency of approximately 47% and very low added noise below one photon based on silicon nanomechanics technology have been reported in Ref.<sup>72</sup>. On the other hand, the technology of SOPDs is now matured, and SOPDs with detection efficiency of up to 90% and low DCR as low as 1 Hz are now available commercially (for instance, see IDQ ID281 SNSPD). Suppose the PDL of the SOPD as its DCR-equivalent power, and consider that the conversion efficiency of the coherent quantum microwave-to-optical transducer is denoted by  $\eta_{\text{trans.}}$ . Then, the PDL for the efficient microwave detection scenario based on the quantum transducer is given by

$$P_{\text{PDL}}^{\text{trans.}} \approx \frac{1}{\eta_Q^{\text{SOPD}} \eta_{\text{trans.}}} h f_s \text{DCR}_{\text{SOPD}}. \quad (58)$$

As an example, by employing the SOPD with  $\eta_Q^{\text{SOPD}} = 0.9$  and  $\text{DCR}_{\text{SOPD}} = 1$  Hz, and the quantum microwave-to-optical transducer with the conversion efficiency of  $\eta_{\text{trans.}} = 0.47$ , one can obtain the PDL using Eq. (58) as  $P_{\text{PDL}}^{\text{trans.}} \approx 1.97 \times 10^{-23}$  W (−197.05 dBm). Figure 9a provides a comparative illustration of the PDL of different microwave detection technologies for better intuition.

Based on the aforementioned analyses, we are now going to evaluate the performance of the quantum-entangled noise radars by considering the restrictions induced by the microwave detection technologies. This allows us to determine the most efficient microwave detection scenario that preserves the advantages provided by quantum-entangled noise radars. To address this, we have to compare the power of the received signal with the PDL of the various microwave detection technologies introduced in this section.

It is obvious that the total number of photons that incident on the receiver antenna is given by

$$N_{\text{inc}} = \langle \hat{a}_{\text{S,inc}}^\dagger \hat{a}_{\text{S,inc}} \rangle, \quad (59)$$

where  $\hat{a}_{\text{S,inc}}$  denotes the annihilation operator of the incident

microwave field and is given as

$$\hat{a}_{\text{S,inc}} = \sqrt{\eta(R)G_{\text{S,tr}}} \hat{a}_{\text{S}} + \sqrt{\eta(R)(G_{\text{S,tr}} - 1)} \hat{c}_{\text{S,tr}}^\dagger + \sqrt{1 - \eta(R)} \hat{a}_{\text{env}}. \quad (60)$$

From Eqs.(59) and (60), one can obtain the total number of photons incident on the radar receiver—including contributions from both the entangled signal and the added noise as follows

$$N_{\text{inc}} = \eta(R)G_{\text{S,tr}}N_s + N_{\text{n,inc}}, \quad (61)$$

where

$$N_{\text{n,inc}} = [1 - \eta(R)]N_{\text{env}} + \eta(R)(G_{\text{S,tr}} - 1)(N_{\text{S,tr}}^{\text{amp}} + 1), \quad (62)$$

represents the total added noise into the incident field. Thus, the corresponding power of the incident field can be calculated as

$$P_{\text{inc}} = h f_s N_{\text{inc}} B_a = P_{\text{S,inc}} + P_{\text{n,inc}}, \quad (63)$$

where  $P_{\text{S,inc}}$  is the power of the back-scattered entangled signal reaching the receiver antenna, and is given by

$$P_{\text{S,inc}} = \eta(R)G_{\text{S,tr}}h f_s N_s B_a. \quad (64)$$

Moreover, the noise power at the antenna  $P_{\text{n,inc}}$  is given by

$$P_{\text{n,inc}} = h f_s N_{\text{n,inc}} B_a. \quad (65)$$

It is crucial to emphasize that the radar receiver must be sensitive to the entangled portion of the incident field, i.e.,  $P_{\text{S,inc}}$ . If the power of this component falls below the PDL, no photocurrent will be generated, and consequently, no information about the target can be extracted.

In Fig. 9b, we have demonstrated the total incident power,  $P_{\text{inc}}$ , alongside the power of the entangled signal,  $P_{\text{S,inc}}$ , that reached the receiver. In this figure, the PDL of various microwave detection scenarios is illustrated. The system parameters used in Fig. 9b are the same as summarized in Table II, with the target RCS as  $\sigma = 0.5$  m<sup>2</sup>. Here, the red, yellow, blue, and green shaded regions correspond to the operational detection regimes for scenarios that utilize the quantum transducer combined with the SOPD, SMPD, the low-temperature and the room-temperature classical antenna, respectively. Incident power below the red-shaded region is undetectable with the current detection technologies.

According to Fig. 9b, for the case where  $N_s = 0.05$ , by employing the room-temperature antenna, the considered system can detect the target with the maximum range of 4.8 m. However, by employing low-temperature classical antennas operating at approximately 30 K, the detection range extends to roughly 8.45 m. Utilizing the state-of-the-art SMPD, such as the one reported in Ref.<sup>42</sup>, the detection range increases up to 1.19 km, an increase of more than 200 times relative to the room-temperature antenna case. In addition, the detection scenario based on the quantum transducer introduced in Ref.<sup>72</sup> enables the detection of weak received signals from the target

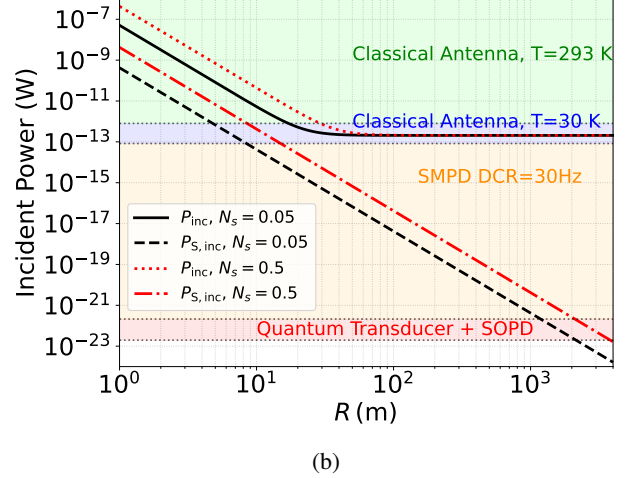
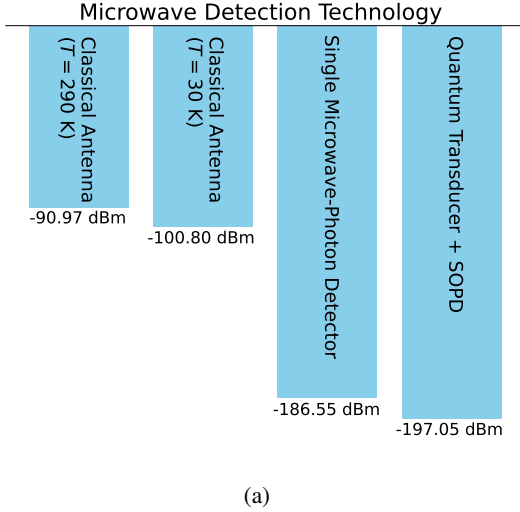


FIG. 9: (Color online) (a) Comparison of the physical detection limit of various microwave detection technologies. (b) The power of the total microwave field (signal + noise) and the signal field incident on the radar receiver as the function of target range  $R$  for the different values of  $N_s$  as 0.05 and 0.5. The system parameters used in this figure are the same as in Table II. The shaded regions indicate the operational regimes of the different microwave detection technologies.

at ranges up to 2.15 km. Here, to obtain these results we have assumed  $N_s = 0.5$ .

It is important to note that the maximum detection range obtained in Eq. (38) assumes an ideal microwave receiver, and did not consider the limitation imposed by the PDL. In order to account this, in addition to the result obtained in Eq. (38), we should consider the range at which the power of the entangled signal at the receiver becomes equivalent to the PDL of the receiver, denoted by  $R_{\text{PDL}}$ . One can obtain this range by solving the equation  $P_{\text{S,inc}} = P_{\text{PDL}}$  for  $R_{\text{PDL}}$ , which yields

$$R_{\text{PDL}} = \frac{20}{\ln(10)\gamma} W_0 \left[ \frac{\ln(10)\gamma}{20} \left( \frac{\sigma G A_e G_{\text{S,tr}} h f_s N_s B_a}{(4\pi)^2 P_{\text{PDL}}} \right)^{1/4} \right]. \quad (66)$$

As a consequence, for a quantum-entangled noise radar, the experimentally achievable detection range is given by

$$R_{\text{max}} \equiv \min \{ R_{\text{max}}^{\text{OI}}, R_{\text{PDL}} \}. \quad (67)$$

Note that to completely exploit the advantages of quantum-entangled noise radars predicted by Eq. (38), the microwave detection technology must satisfy the condition  $R_{\text{PDL}} \geq R_{\text{max}}^{\text{OI}}$ . Therefore, an efficient microwave detection scenario for a quantum-entangled noise radar is that for which this condition is satisfied. Otherwise, the detection range is limited to  $R_{\text{PDL}}$ , which results in a reduction of the REF compared to its classical counterpart. However, it may still be capable of detecting targets at kilometer-range distances.

## 2. Application-Specific Suitability

Experimental implementations of quantum-entangled noise radars have been restricted to operation inside controlled lab-

oratory environments. Up to now, no practical systems have been realized for specific real-world applications yet. To provide a perspective on potential deployments in the future, we have plotted the maximum detection range of the quantum-entangled noise radar in terms of the target RCS in Fig. 10. The system parameters are the same as listed in Table II with  $N_s = 0.05$ . Here, the schematic icons representing different targets (i.e., insect, stealth aircraft, bird, commercial drone, human body, and light aircraft) are included to provide a quick visual sense for readers. Moreover, the parameter  $R_{\text{PDL}}$  for the microwave detection technologies based on the quantum transducer and SMPD are illustrated by the red dot-dashed and green dotted curves, respectively.

As shown in Fig. 10, in the search mode with  $P_{\text{fa}} = 0.1$ , the maximum detection range predicted by Eq. (38) exceeds  $R_{\text{PDL}}$  when employing the detection scenario based on the quantum transducer. Consequently, as indicated by Eq. (67), the maximum achievable detection range is constrained by  $R_{\text{PDL}}$ . However, the difference between the two is negligible. In the track mode with  $P_{\text{fa}} = 0.001$ , the maximum detection range predicted by Eq. (38) remains below  $R_{\text{PDL}}$  for the same detection scenario. Therefore, in the track mode, Eq. (38) accurately describes the achievable detection range of the considered quantum-entangled noise radar. In contrast, for the detection scenario that utilizes the SMPD, the parameter  $R_{\text{PDL}}$  is significantly lower than the range predicted by Eq. (38) in both the search and track modes. As a result, the ultimate detection range in this case is determined by  $R_{\text{PDL}}$ . Consequently, even with the state-of-the-art SMPDs featuring a DCR as low as 30 Hz<sup>42</sup>, the system performance is significantly restricted. As illustrated in Fig. 9a, classical antennas, even when cooled to low temperatures, exhibit  $R_{\text{PDL}} \simeq 8.45$  m, which is substantially lower than the maximum detection range predicted by Eq. (38). This discrepancy effectively nullifies the advantages

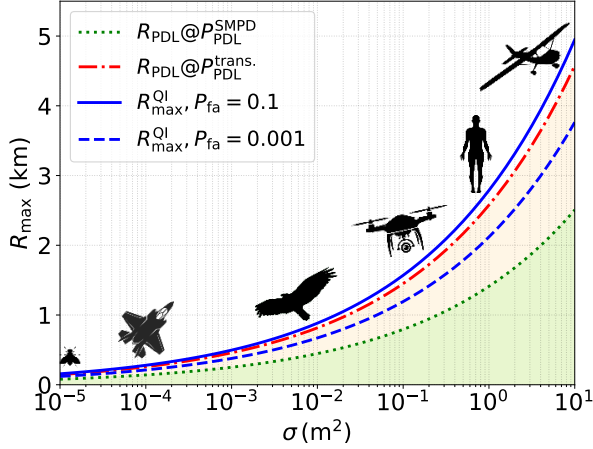


FIG. 10: (Color online) The maximum detection range of the quantum-entangled noise radar,  $R_{\max}^{\text{QI}}$ , in terms of the object's RCS,  $\sigma$ , for  $N_s = 0.05$ . The other system parameters are the same as in Table. II.

of quantum-entangled radar systems. This may explain the limited range, of approximately 1 m, of the quantum-entangled radar system implemented in Ref.<sup>59</sup>.

In summary, to effectively employ the performance advantages offered by quantum-entangled noise radars, the use of a microwave detection system based on the quantum transducer combined with a high-efficiency SOPD is strongly recommended. It should be noted that the following analysis is based on the assumption of using the quantum transducer-based microwave detection technology.

Figure 10 demonstrates that the considered quantum-entangled noise radar can detect a stealth aircraft with an RCS around  $\sigma \approx 10^{-4} \text{ m}^2$  at ranges up to 271 m (206 m) in the search (track) mode. A typical stealth aircraft travels at speeds of 200 – 700 m/s. By considering the minimum warning time required for its detection as 60 seconds, then the necessary detection range is obtained to be 12 – 42 km, which greatly exceeds the quantum-entangled radar's maximum detection range. Consequently, the current quantum-entangled noise radar configuration is inadequate for early-warning applications for high-speed stealth aircraft.

However, for typical commercial drones with an RCS of the order of  $\sigma \approx 0.5 \text{ m}^2$  and moderate speeds of approximately 20 – 30 m/s, the maximum detection range of the considered quantum-entangled noise radar is approximately 2.28 km in the search mode and 1.7 km in the track mode. It is comparable to or exceeds the required warning distance for such targets. Therefore, the quantum-entangled noise radar under investigation could be suitable for detecting and tracking common commercial drones in real-world applications.

For a light aircraft with typical speeds of 60 – 70 m/s and an RCS of approximately  $\sigma \approx 10 \text{ m}^2$ , the maximum detection range of the quantum-entangled noise radar is 4.8 km in the search mode and 3.65 km in the track mode. This performance is marginally consistent with the operational range of

precision approach radars (PAR) used at airports. Accordingly, quantum-entangled noise radars may have potential applications in airport surveillance systems.

Regarding the other targets illustrated in Fig. 9, such as birds and humans, the quantum-entangled noise radar demonstrates acceptable maximum detection ranges. Consequently, potential applications for quantum-entangled noise radars include radar-based non-contact human vital sign detection<sup>66</sup> as well as studies in aeroecology and aerobiology<sup>67</sup>.

In this study, we have focused solely on evaluating the operational performance of the quantum-entangled noise radar based on the current state-of-the-art technologies. The system performance has been examined for specific applications to assess their suitability, without considering practical challenges such as implementation complexity, cost, size, weight, and power consumption (SWaP)<sup>68,69</sup>. These practical issues are beyond the scope of the present work and warrant comprehensive analysis tailored to each individual application.

### 3. Entanglement in Quantum-Entangled Noise Radars

We are now going to revisit the challenge concerning the entanglement between the back-scattered signal from the target at a range  $R$  and the retained idler. In order to address this issue, one needs to evaluate an appropriate entanglement measure between the signal and idler modes. Here, Simon's separability criterion is employed for this purpose. As demonstrated in Appendix B, the signal and idler modes generated at the source, represented by Eq. (22), are shown to be inseparable (i.e., entangled) for any photon number per mode  $N_s > 0$ . Nonetheless, it vanishes due to signal amplification, free-space propagation, and detection at the receiver (cf. Appendix B). This observation raises an important question: if the quantum entanglement is sufficiently fragile and completely destroyed during the free-space propagation, what then underlies the advantage of the quantum-entangled noise radars over the classical ones?

To clarify the apparent paradox, it must be remembered that the absence of entanglement is not equivalent to classicality<sup>73</sup>. As the initial entanglement is entirely eradicated during propagation through the free-space channel, the quantum advantage might still persist due to the presence of quantum correlations beyond entanglement. Particularly, it can be attributed to quantum discord, which is a more robust quantum correlation than entanglement. Thus, the quantum discord can be seen as a quantum resource of quantum correlation in such scenarios<sup>73</sup>.

Quantum discord is defined as the difference between the total correlations within a quantum state, as quantified by the quantum mutual information, and the classical correlations of that state. It corresponds to the maximum amount of shared randomness accessible via local measurements and one-way classical communication<sup>74,75</sup>. In essence, the residual quantum correlations that remain despite the loss of entanglement are responsible for the improved performance of entanglement-based target detection schemes versus the classical target detection.

#### IV. SUMMARY, CONCLUSION REMARKS AND OUTLOOKS

In this paper, we have presented an analysis of the operational performance of the quantum single-photon direct-detection radars (see Sec. II) and quantum-entangled noise radars (see Sec. III), focusing on their maximum detection range. For both radar types, we have calculated the explicit expressions for the maximum detection range in terms of the Lambert W function. Our analysis has provided a comprehensive model that incorporates all the relevant system and environmental parameters.

Analogous to single-photon LiDAR systems, we have explored the feasibility of employing single microwave-photon detectors as the radar receiver to realize single-photon radar systems. Based on recent advances in SMPD technology, we have demonstrated that implementing a single-photon radar with the transmit power of the order of a few milli-watts and the detection range in the order of a few kilometers is feasible (see Sec. II). This development holds promise for the realization of low-power, high-performance single-photon radar systems for practical field applications. Nevertheless, further advancement and optimization of SMPD technology is necessary to achieve this goal.

In the case of quantum-entangled noise radars, we have derived an explicit expression for the maximum detection range in terms of the Lambert W function. This allows us to define an effective threshold SNR for quantum-entangled noise radars (see Eq. (37)). This suggests that a noise radar can be interpreted effectively as a direct-detection radar with a reduced threshold SNR.

To demonstrate the performance advantage of quantum-entangled noise radars with respect to their classical counterparts, we have also introduced the REF parameter. We have also derived a rule-of-thumb approximation for the REF in terms of the quantum advantage  $Q_{\text{adv}}$ , which depends solely on the mean photon number per mode,  $N_s$  (see Eq. (50)). Moreover, we have linked REF to SNR enhancement from the engineering point of view. In addition, we have classified the quantum-entangled noise radars into two operational modes based on the false-alarm probability: the search and track modes.

In this paper, a quantitative evaluation of the maximum detection range is provided using feasible system parameters based on the current state-of-the-art technologies (see Table II). Our results show that the quantum-entangled noise radars have the potential to detect small targets with the RCS  $\sigma = 0.1 \text{ m}^2$  up to a range of 2 km in the track mode with  $P_{\text{fa}} = 0.001$ . More importantly, we have shown that the target detection occurs within a reasonable integration time, and the system shows a substantial range enhancement factor of  $\text{REF} = 2.14$  (see Fig. 8). We have also compared the chosen system parameters with those reported in some of the most notable experimental implementations of the quantum-entangled noise radars to date (see Table III). This comparison demonstrates that our considered system parameters are achievable via current technologies.

Additionally, we have addressed several practical chal-

lenges related to the operation and application of the quantum-entangled noise radars (see Subsec. III E). In particular, we have explored the potential use of these radars for detecting various targets, such as stealth aircraft, birds, commercial drones, human bodies, and light aircraft. For stealth aircraft, by comparing the radar's maximum detection range with the minimum warning range required for such high-speed and low-RCS targets, one can conclude that quantum-entangled noise radars under current technological constraints are not yet suitable for this application. However, they have strong potential for detecting commercial drones at urban distances. Furthermore, they might be used as precision approach radars in airports (see Fig. 9).

By considering the inherently low power of the transmitted entangled signal in quantum-entangled noise radars, we have also examined whether the power of the back-scattered signal is sufficient for detection with current radar receivers. To this end, we have compared the received signal power with the physical detection limit of modern microwave receiver antennas and state-of-the-art SMPDs. Our analysis shows that, for instance, the maximum range at which the received signal power reaches the PDL is approximately 2.23 km for  $N_s = 0.5$ . To overcome this limitation, one can use high-efficiency quantum microwave-to-optical transducers, such as those based on quantum electro-optomechanical systems<sup>77</sup>, to coherently convert the back-scattered microwave signals into optical ones. This approach employs highly efficient SOPDs for detecting optical signals.

From an engineering and practical standpoint, several key directions can be pursued to achieve long-range quantum-entangled noise radars as follows:

- *Broadband entangled microwave sources*: Increasing the operational bandwidth of entangled microwave sources is essential for enhancing both the maximum detection range and quantum advantage. This can be achieved through platforms based on electro-optomechanical (EOM) systems, superconducting circuits, or spin-based systems such as nitrogen-vacancy centers.
- *Photonics-based radar platforms*: Integrating quantum-entangled noise radar architectures with photonic radar systems can facilitate more efficient signal detection and post-processing<sup>76</sup>. High-efficiency quantum *microwave-to-optics transducers*—such as EOM-based transducers<sup>77</sup>—and efficient RF antennas designed specifically for the emission of entangled microwave signals in open-air<sup>78</sup> are critical for enabling this integration.
- *Room-temperature entanglement sources*: Generating entangled microwave signals at ambient or high temperatures is possible through utilizing advanced EOM platforms<sup>79,80</sup> or superconducting systems<sup>81</sup> via quantum control techniques. Exploring bulk or integrated nonlinear optical crystals<sup>82–84</sup>, NV centers<sup>85</sup>, or other room-temperature quantum sources could eliminate the need for cryogenic systems. Utilizing high-temperature microwave photon-pair sources can significantly reduce system SWaP and cost.

- *Single microwave-photon detectors*: The development of low DCR, high-sensitivity single microwave photon detectors—especially those that can operate at higher temperatures<sup>86–88</sup>—would substantially reduce the effective threshold SNR which enhances the radar performance.
- *Investigate quantum-entangled noise radars based on non-Gaussian entangled states*: The analysis of the maximum detection range presented in this work is restricted to the use of quantum two-mode Gaussian states to generate the correlated signal and idler fields<sup>89,90</sup>. It seems that employing non-Gaussian quantum entangled states may enhance the quantum advantage and also further increase the maximum detection range.

## AUTHOR CONTRIBUTION

AMF as the corresponding author and director of the quantum sensing & metrology Lab/group at ICQT has defined and led this project. All calculations have been done by HA and rechecked and interpreted by AMF. All numerical calculations and graphs have been plotted by HA. The subjects of the quantum antenna or single-photon microwave detectors for improving the threshold-SNR have been introduced and developed by AMF. The effective-SNR has been defined and developed by HA and has been interpreted by AMF. AMF introduced and developed the engineering parameters and approaches such as REF and so on, and then, HA checked and re-formulated them. Experimental parameters have been determined and extracted by both authors. Both authors have contributed to the discussion and interpretation of the results as well as writing, editing and revising the manuscript. The idea of investigating the received photon number and Simon criterion are put forwarded by AMF, calculated by HA and then re-checked by AMF. Both authors contributed to answer to the reviewers, and prepare the response letter.

## ACKNOWLEDGMENTS

The authors thank the Iranian Center for Quantum Technologies (ICQT). AMF would thank the University of Tehran.

## AUTHOR DECLARATIONS

### Conflict of Interest

The authors have no conflicts to disclose.

## DATA AVAILABILITY STATEMENT

This study is entirely theoretical in nature. No experimental data were generated or analyzed, and thus no data are available for public access.

## Appendix A: Squeezing origination of microwave QTMS state in JPA

It is well-known that in the optical domain, the entangled Gaussian states can be generated by the SPDC, a 3-wave mixing process in NLCs in which a pump photon with the higher energy is converted through the second-order nonlinear interaction with quantum vacuum fluctuations into a pair of signal-idler photons with the lower energy respecting the energy-momentum conservation law. Since signal-idler biphoton is created from the same quantum vacuum, they both share entanglement between each other stronger than any classical correlation. On the other hand, in the microwave band, phase-preserving JPAs, as a quantum-limited amplifiers that operate in 3-10GHz band with signal-idler frequency which can be adjusted in GHz-band, are responsible for the microwave entanglement generation via the well-known 4-wave mixing process<sup>92</sup>. In a JPA, two input vacuum signal ports ( $\hat{v}, \hat{\mu}$ ) are mixed together and two amplified sideband signal and idler with power gain  $G_{\text{JPA}}$  are generated. The generation of entanglement from uncorrelated vacuum noise inputs in a JPA can be modeled as<sup>92</sup>

$$\hat{a}_s = \cosh(r)\hat{v} + \sinh(r)\hat{\mu}^\dagger, \quad (\text{A1})$$

$$\hat{a}_i = \sinh(r)\hat{v}^\dagger + \cosh(r)\hat{\mu}, \quad (\text{A2})$$

where  $r$  is referred to the squeezing parameter and is related to the amplification gain power as  $G_{\text{JPA}} = \cosh^2(r)$ . It is simple to show that the signal-idler quadratures of a QTMS state is a zero-mean Gaussian thermal state with average photon number as the so-called photon per mode  $N_s = [\cosh(2r) - 1]/2$  which immediately implies that signal-idler correlation in the Covariance matrix becomes  $\mathcal{C}_Q = \sinh(2r)/2$  which can be greater than its classical counterpart. Surprisingly, this quantum advantage is responsible for the noise reduction below the quantum vacuum ( $1/2$ ) in generalized quadratures  $\hat{I}_- = (\hat{I}_s - \hat{I}_i)/\sqrt{2}$  and  $\hat{Q}_+ = (\hat{Q}_s + \hat{Q}_i)/\sqrt{2}$ . This leads to quadrature squeezing as follows

$$\text{Var}[\hat{I}_-] = e^{-2r}/2, \quad (\text{A3})$$

which has been experimentally realized up to around -12dB<sup>93</sup>.

## Appendix B: Simon's Separability Criterion

Here, in this appendix we are going to calculate the Simon's separability criterion for the signal and idler modes before the transmission of the signal and also after returning the back-scattered signal from the target to the receiver in general situation by considering attention, amplification and noise. To this, we starts with the covariance matrix for the signal and idler modes at the transmitter which is given by<sup>94</sup>

$$\text{Cov}_{\text{tr}} = \frac{1}{4} \begin{pmatrix} S_1 & 0 & C_q & 0 \\ 0 & S_1 & 0 & -C_q \\ C_q & 0 & S_2 & 0 \\ 0 & -C_q & 0 & S_2 \end{pmatrix}, \quad (\text{B1})$$

where  $S_1 = S_2 = 2N_s + 1$ , and  $C_q = \sqrt{N_s(N_s + 1)}$ . By utilizing the annihilation operator of the detected idler and signal fields given in Eqs. (14) and (21), the covariance matrix for the detected signal and idler fields is obtained as

$$\text{Cov}_{\text{rec}} = \frac{1}{4} \begin{pmatrix} S'_1 & 0 & C'_q & 0 \\ 0 & S'_1 & 0 & -C'_q \\ C'_q & 0 & S'_2 & 0 \\ 0 & -C'_q & 0 & S'_2 \end{pmatrix}, \quad (\text{B2})$$

with

$$S'_1 = 2[\eta G_{\text{S}} N_s + G_{\text{S,rec}} N_{\text{env}} + G_{\text{S,rec}} (G_1 - 1)(N_{\text{S,tr}}^{\text{amp}} + 1) + (G_{\text{S,rec}} - 1)(N_{\text{S,rec}}^{\text{amp}} + 1)] + 1, \quad (\text{B3})$$

$$S'_2 = 2[G_1 N_s + (G_1 - 1)(N_1^{\text{amp}} + 1)] + 1 \quad (\text{B4})$$

$$C'_q = \sqrt{\eta G_{\text{S}}^{\text{amp}} G_1^{\text{amp}} C_q}, \quad (\text{B5})$$

The parameters in these relations have previously defined in Sec. III. It is worth noting that when there is no amplification, i.e.,  $G_{\text{S,rec}} = G_1 = 1$ , the covariance matrix given in Eq. (B2) reduces to that reported in references<sup>91,94</sup> for QTMS radar with no amplification.

As mentioned in Ref.<sup>94</sup>, the entanglement between the signal and idler mode can be evaluated through the so-called Simon's separability criterion as

$$f \geq 0, \quad (\text{B6})$$

in which  $f$  is defined as Simon parameter, and for the signal and idler modes represented by the covariance matrix of the form (B1) or (B2) is defined as

$$f \equiv (S_1 S_2 - C_q^2)^2 - (S_1^2 + S_2^2 + 2C_q^2) + 1. \quad (\text{B7})$$

Using this equation, it is straightforward to show that  $f$  at the source is given by

$$f_{\text{source}} = -16N_s(N_s + 1), \quad (\text{B8})$$

which is negative for any  $N_s > 0$ . Therefore, it is concluded that the generated signal and idler modes are inseparable or entangled. However, using Eq. (B3)-(B5) one can obtain  $f$  for the detected signal and idler modes as

$$f_{\text{det}} = (S'_1 S'_2 - C_q'^2)^2 - (S_1'^2 + S_2'^2 + 2C_q'^2) + 1. \quad (\text{B9})$$

By considering  $G_1 = 77$  dB,  $G_{\text{S,rec}} = 17$  dB, and the other system parameters as the same as reported in Table. (II), one finds that  $f_{\text{det}} \gg 1$  for any  $R > 0$ . Therefore, the detected signal and idler modes are not entangled, and what is help us to exploit the entanglement is quantum discord as the quantum resource of residual quantum correlation.

<sup>1</sup>M. Guarnieri, "The Early History of Radar [Historical]," IEEE Ind. Electron. Mag., vol. 4, no. 3, pp. 36-42, Sept. 2010, DOI 10.1109/MIE.2010.937936.

<sup>2</sup>Drake, V. Alistair, and Donald Russell Reynolds, "Radar entomology: observing insect flight and migration," Cabi, 2012.

<sup>3</sup>B. J. Jang, S. H. Wi, J. G. Yook, M. Q. Lee, and K. J. Lee, "Wireless bio-radar sensor for heartbeat and respiration detection," Prog. Electromagn. Res. C, vol. 5, pp. 149-168, Dec. 2008, DOI 10.2528/PIERC08110603.

<sup>4</sup>L. Creed, J. Graham, C. Jenkins, S. Diaz-Riofrio, A. Wilson, and M. Vasile. (2021, October) STRATHcube: the design of a CubeSat for space debris detection using in-orbit passive bistatic radar. presented at 72nd International Astronautical Congress.

<sup>5</sup>Kyle J. Kauffman, "Radar based navigation in unknown terrain," Air Force Institute of Technology, 2012.

<sup>6</sup>S. Bauer, J. W. Chapman, D. R. Reynolds, J. A. Alves, A. M. Dokter, M. M. H. Menz, N. Sapir, M. Ciach, L. B. Pettersson, J. F. Kelly, H. Leijnse, J. Shamoun-Baranes, "From agricultural benefits to aviation safety: realizing the potential of continent-wide radar networks," BioScience, vpl. 67, no. 10, pp. 912-918, Jun. 2017, DOI 10.1093/biosci/bix074.

<sup>7</sup>E. Morganti, L. Angelini, A. Adami, D. Lalanne, L. Lorenzelli, E. Mugellini, "A smart watch with embedded sensors to recognize objects, grasps and forearm gestures," Proc. Eng., vol. 41, pp. 1169-1175, 2012, DOI 10.1016/j.proeng.2012.07.297.

<sup>8</sup>Merrill I. Skolnik, "Radar handbook," McGraw-Hill Education, 2008.

<sup>9</sup>R. M. Narayanan, Y. Xu, P. D. Hoffmeyer, and J. O. Curtis, "Design, performance, and applications of a coherent ultra-wideband random noise radar," Opt. Eng., vol. 37, no. 6, pp. 1855-1869, Jun. 1998, DOI 10.1117/1.601699.

<sup>10</sup>Konstantin A. Lukin, "Noise radar technology," Telecom. Rad. Eng., vol. 55, no. 12, 2001, DOI 10.1615/TelecomRadEng.v55.i12.20.

<sup>11</sup>K. Savci, A. G. Stove, F. De Palo, A. Y. Erdogan, G. Galati, K. A. Lukin, S. Lukin, P. Marques, G. Pavan, C. Wasserzler, "Noise Radar? Overview and Recent Developments," IEEE Aerosp. Electron. Syst. Mag., vol. 35, no. 9, pp. 8-20, Sept. 2020, DOI 10.1109/MAES.2020.2990591.

<sup>12</sup>D. Massaro, R. Ardoino, and M. Grazzini, "An Efficient Processing Architecture for Range Profiling Using Noise Radar Technology," Aerospace, vol. 5, no. 1, Jan. 2018, DOI 10.3390/aerospace5010004.

<sup>13</sup>Torromé, Ricardo Gallego and Barzanjeh, Shabir, "Advances in quantum radar and quantum LiDAR," Prog. Quant. Electron., pp. 100497, 2023, DOI 10.1016/j.pquantelec.2023.100497.

<sup>14</sup>Shapiro, Jeffrey H., "The quantum illumination story," IEEE Aerosp. Electron. Syst. Mag., vol. 35, no. 4, pp. 8-20, 2020, DOI 10.1109/MAES.2019.2957870.

<sup>15</sup>Pirandola, Stefano, B. Roy Bardhan, Tobias Gehring, Christian Weedbrook, and Seth Lloyd, "Advances in photonic quantum sensing," Nat. Photonics, vol. 12, no. 12, pp. 724-733, 2018, DOI 10.1038/s41566-018-0301-6.

<sup>16</sup>S. Lloyd, "Enhanced sensitivity of photodetection via quantum illumination," Science, vol. 321, no. 5895, pp. 1463-1465, 2008, DOI 10.1126/science.1160627.

<sup>17</sup>E. D. Lopaeva, I. R. Berchera, I. P. Degiovanni, S. Olivares, G. Brida, and M. Genovese, "Experimental realization of quantum illumination," Phys. Rev. Lett., vol. 110, no. 15, pp. 153603, 2013, DOI https://doi.org/10.1103/PhysRevLett.110.153603.

<sup>18</sup>Sh. Barzanjeh, S. Guha, Ch. Weedbrook, D. Vitali, J. H. Shapiro, and S. Pirandola, "Microwave quantum illumination," Phys. Rev. Lett., vol. 114, no. 8, pp. 080503, 2015, DOI https://doi.org/10.1103/PhysRevLett.114.080503.

<sup>19</sup>D. Luong, B. Balaji, C. W. Sandbo Chang, W. M. Ananthapadmanabha Rao and C. Wilson, "Microwave Quantum Radar: An Experimental Validation," In 2018 International Carnahan Conference on Security Technology (ICCST), Montreal, QC, Canada, 2018, pp. 1-5.

<sup>20</sup>B. Balaji, "Quantum radar: Snake oil or good idea?," In 2018 International Carnahan Conference on Security Technology (ICCST), Montreal, QC, Canada, 2018, pp. 1-7.

<sup>21</sup>Ph. S. Blakey, H. Liu, G. Papangelakis, Y. Zhang, Z. M. Leger, M. L. Iu, and A. S. Helmy, "Quantum and non-local effects offer over 40dB noise resilience advantage towards quantum lidar," Nat. Commun., vol. 13, no. 1, pp. 5633, 2022, DOI https://doi.org/10.1038/s41467-022-33376-9.

<sup>22</sup>H. Liu, Ch. Qin, G. Papangelakis, M. L. Iu, and A. S. Helmy, "Compact all-fiber quantum-inspired LiDAR with over 100dB noise rejection and single photon sensitivity," Nat Commun., vol. 14, no. 1, pp. 5344, 2023, DOI https://doi.org/10.1038/s41467-023-40914-6.

<sup>23</sup>M. Reichert, R. Di Candia, M. Z. Win, M. Sanz, "Quantum-enhanced Doppler lidar," npj Quantum Inf., vol. 8, no. 1, pp. 147, 2022.

<sup>24</sup>R. J. Murchie, J. D. Pritchard and J. Jeffers, "Object detection and ranging with quantum states using simple detection," arXiv:2307.10785v3 [quant-ph], 2023.

<sup>25</sup>M. P. Mrozowski, R. J. Murchie, J. Jeffers, and J. D. Pritchard, "Demonstration of quantum-enhanced ranging robust against clas-

- sical jamming," *Opt. Exp.*, vol. 32, no. 3, pp. 1916-2928, 2024, DOI <https://doi.org/10.1364/OE.503619>.
- <sup>26</sup>M. Huang, Zh. Jiang, Ho. Chen, Y. Zuo, X. Hu, H. Yuan, L. Zhang, and Q. Qin, "Quantum LiDAR with Frequency Modulated Continuous Wave," arXiv:2307.11590v1 [quant-ph], 2023.
- <sup>27</sup>D. Wang, J. Zhao, Y. Wang, L. Zhou, and Y. Zhao, "Quantum secured LiDAR with Gaussian modulated coherent states," arXiv:2308.12171v1 [quant-ph], 2023.
- <sup>28</sup>R. Murray, and A. Lyons, "Two-photon interference LiDAR imaging," *Opt. Exp.*, vol. 30, no. 15, pp. 27164-27170, 2022, DOI <https://doi.org/10.1364/OE.461248>.
- <sup>29</sup>Thomas Brougham, Nigam Samantary, and John Jeffers, "Using random coherent states to mimic quantum illumination," *Phys. Rev. A*, vol. 108, no. 5, pp. 052404, Nov. 2023, DOI <https://doi.org/10.1103/PhysRevA.108.052404>.
- <sup>30</sup>A. Karsa, G. Spedalieri, Q. Zhuang, and S. Pirandola, "Quantum illumination with a generic Gaussian source," *Phys. Rev. Res.*, vol. 2, no. 2, pp. 023414, June. 2020, DOI 10.1103/PhysRevResearch.2.023414.
- <sup>31</sup>S. Barzanjeh, S. Pirandola, D. Vitali, and J. M. Fink "Microwave quantum illumination using a digital receiver," *Sci. Adv.*, vol. 6, no. 19, pp. eabb0451, May. 2020, DOI 10.1126/sciadv.abb0451.
- <sup>32</sup>D. Luong, I. W. K. Lam, B. Balaji, and S. Rajan, "Correlation Coefficient vs. Transmit Power for an Experimental Noise Radar," In 2023 IEEE Radar Conference (RadarConf23), San Antonio, TX, USA, 2023, pp. 1-5.
- <sup>33</sup>P. Livreri, E. Enrico, D. Vitali, and A. Farina, "Microwave Quantum Radar using a Josephson Traveling Wave Parametric Amplifier and a Phase-Conjugate Receiver for a long-distance detection," 2023 IEEE Radar Conference (RadarConf23), San Antonio, TX, USA, 2023, pp. 1-5.
- <sup>34</sup>P. Livreri, E. Enrico, L. Fasolo, G. Di Giuseppe, N. Malossi, P. Piergentili, and D. Vitali, "Microwave Quantum Radar based on a Josephson Traveling wave Parametric Amplifier and a Phase-Conjugate Receiver," *TechRxiv.21778007.v1*, 2022.
- <sup>35</sup>D. Luong, B. Balaji and S. Rajan, "Performance Prediction for Coherent Noise Radars Using the Correlation Coefficient," *IEEE Access*, vol. 10, pp. 8627-8633, 2022, DOI 10.1109/ACCESS.2021.3135292.
- <sup>36</sup>R. Wei, J. Li, W. Wang, Zh. Ye, Ch. Zhao, and Q. Guo, "Evaluating the detection range of microwave quantum illumination radar," *IET Radar. Sonar. Nav.*, vol. 17, no. 11, pp. 1664-1673, Aug. 2023, DOI <https://doi.org/10.1049/rns2.12456>.
- <sup>37</sup>F. Bischeltsrieder, M. Würth, J. Russer, M. Peichl, and W. Utschick, "Engineering Constraints and Application Regimes of Quantum Radar," *IEEE Trans. Radar Syst.*, vol. 2, pp. 197-214, Feb. 2024, DOI 10.1109/TRS.2024.3361048.
- <sup>38</sup>P. Livreri, B. Galvano, L. Fasolo, L. Oberto, E. Enrico, "Josephson Traveling Wave Parametric Amplifier as Quantum Source of Entangled Photons for Microwave Quantum Radar Applications," *ELECTROMAGNETIC WAVES*, vol. 179, pp. 113-124, 2024, DOI <https://dx.doi.org/10.2528/pier24041705>.
- <sup>39</sup>M. Ankel, R. Jonsson, T. Bryllert, L. M. H. Ulander, and P. Delsing, "Bistatic noise radar: Demonstration of correlation noise suppression," *IET Radar. Sonar. Navigation*, vol. 17, no. 3, pp. 351, Nov. 2023, DOI <https://doi.org/10.1049/rns2.12345>.
- <sup>40</sup>R. M. Corless, G. H. Gonnet, D. EG. Hare, D. J. Jeffrey, and D.E. Knuth, "On the Lambert W function," *Advances in Computational mathematics*, vol. 5, pp. 329-359, 1996, DOI <https://doi.org/10.1007/BF02124750>.
- <sup>41</sup>O. Steinvall, "Laser system range calculations and the Lambert W function," *Applied Optics*, vol. 48, pp. B1-B7, 2008, DOI <https://doi.org/10.1364/AO.48.0000B1>.
- <sup>42</sup>L. Pallegoix, J. Travesedo, A. S. May, L. Balembois, D. Vion, P. Bertet, E. Flurin, "Enhancing the sensitivity of single microwave photon detection with bandwidth tunability," arXiv preprint arXiv:2501.07354 2025, DOI <https://doi.org/10.48550/arXiv.2501.07354>
- <sup>43</sup>L. Balembois, J. Travesedo, L. Pallegoix, A. May, E. Billaud, M. Villiers, D. Estève, D. Vion, P. Bertet, E. Flurin, "Cyclically operated microwave single-photon counter with sensitivity of  $10^{-22} \text{W}/\sqrt{\text{Hz}}$ " *Physical Review Applied*, vol. 21, pp. 014043, 2024, DOI <https://doi.org/10.1103/PhysRevApplied.21.014043>
- <sup>44</sup>R. Dassonneville, R. Assouly, T. Peronnin, P. Rouchon, B. Huard, "Number-resolved photocounter for propagating microwave mode" *Physical Review Applied*, vol. 14, pp. 044022, 2020, DOI <https://doi.org/10.1103/PhysRevApplied.14.044022>.
- <sup>45</sup>K. Inomata, Z. Lin, K. Koshino, W. D. Oliver, J. S. Tsai, T. Yamamoto, Y. Nakamura, "Single microwave-photon detector using an artificial  $\Lambda$ -type three-level system" *Nature communications*, vol. 7, pp.12303, 2016, DOI 10.1038/ncomms12303.
- <sup>46</sup>F. Oppliger, W. Jang, A. Tarascio, F. De Palma, C. Reichl, W. Wegscheider, V. F. Maisi, D. Zumbühl, and P. Scarlino, "High-Efficiency Tunable Microwave Photon Detector Based on a Semiconductor Double Quantum Dot Coupled to a Superconducting High-Impedance Cavity" arXiv preprint arXiv:2506.19828, 2025, DOI arXiv preprint arXiv:2506.19828.
- <sup>47</sup>K. Petrovnin, J. Wang, M. Perelshtein, P. Hakonen, and G. S. Paraoanu, "Microwave photon detection at parametric criticality" *PRX Quantum*, vol. 5, pp.020342, 2024, DOI <https://doi.org/10.1103/PRXQuantum.5.020342>.
- <sup>48</sup>K. Liu, C. Luo, J. Yi, and H. Wang, "Target detection method using heterodyne single-photon radar at terahertz frequencies" *IEEE Geoscience and Remote Sensing Letters*, vol. 19, pp.1-5, 2021, DOI 10.1109/LGRS.2021.3070546.
- <sup>49</sup>Zh.-P. Li, J.-T. Ye, X. Huang, P. Jiang, Y. Cao, Y. Hong, Ch. Yu, J. Zhang, Q. Zhang, Ch.-Zh. Peng, F. Xu, and J.-W. Pan, "Single-photon imaging over 200 km," *Optica*. vol. 8, no.3, pp. 344-349, 2021, DOI <https://doi.org/10.1364/OPTICA.408657>.
- <sup>50</sup>L. M. Hirvonen and K. Suhling, "Wide-field TCSPC: methods and applications" *Measurement Science and Technology*, vol. 28, no. 1, pp.012003, 2016, DOI 10.1088/1361-6501/28/1/012003.
- <sup>51</sup>P. Series "Attenuation by atmospheric gases and related effects," *Rec. ITU-R*, vol. 25, pp. 676-12, 2019.
- <sup>52</sup>D. Luong, S. Rajan and B. Balaji, "Entanglement-Based Quantum Radar: From Myth to Reality," *IEEE Aerospace and Electronic Systems Magazine*, vol. 35, no. 4, pp. 22-35, 2020, DOI 10.1109/MAES.2020.2970261.
- <sup>53</sup>C. W. Sandbo Chang, A. M. Vadiraj, J. Bourassa, B. Balaji and C. M. Wilson, "Quantum-enhanced noise radar," *Appl. Phys. Lett.* vol. 114, no. 11, 2019, DOI <https://doi.org/10.1063/1.5085002>.
- <sup>54</sup>G. Sorelli, N. Treps, F. Grosshans and F. Boust, "Detecting a Target With Quantum Entanglement," *IEEE Aerospace and Electronic Systems Magazine*.vol. 37, no. 5, pp. 68-90, 2022, DOI 10.1109/MAES.2021.3116323.
- <sup>55</sup>M. Dawood and R. M. Narayanan, "Receiver operating characteristics for the coherent UWB random noise radar," *IEEE Transactions on Aerospace and Electronic Systems*, vol. 37, no. 2, pp. 586-594, 2021, DOI 10.1109/7.937470.
- <sup>56</sup>R. W. Boyd, G. S. Agarwal, W. V. Davis, A. L. Gaeta, E. M. Nagasako, and M. Kauranen, "Quantum noise characteristics of nonlinear optical amplifiers," *Acta Physica Polonica A*, vol. 86, no. 1, pp. 117-126, 1994.
- <sup>57</sup>S. Guha, B. I. Erkmen, "Gaussian-state quantum-illumination receivers for target detection," *Physical Review A—Atomic, Molecular, and Optical Physics*, vol. 80, pp. 052310, 2009, DOI <https://doi.org/10.1103/PhysRevA.80.052310>.
- <sup>58</sup>M. Frasca and A. Farina, "Entangled coherent states for quantum radar applications," 2020 IEEE International Radar Conference (RADAR), Washington, DC, USA, 2020, pp. 969-972.
- <sup>59</sup>D. Luong, C. W. Sandbo Chang, A. M. Vadiraj, A. Damini, C. M. Wilson, and B. Balaji "Receiver operating characteristics for a prototype quantum two-mode squeezing radar," *IEEE Transactions on Aerospace and Electronic Systems*, vol. 56, no. 3, pp. 2041-2060, 2019, DOI 10.1109/TAES.2019.2951213.
- <sup>60</sup>D. Luong, S. Rajan and B. Balaji, "Estimating Correlation Coefficients for Quantum Radar and Noise Radar: A Simulation Study," 2019 IEEE Global Conference on Signal and Information Processing (GlobalSIP), Ottawa, ON, Canada, 2019, pp. 1-5.
- <sup>61</sup>D. Makarov, "Theory for the beam splitter in quantum optics: Quantum entanglement of photons and their statistics, HOM effect," *Mathematics*, vol. 10, no. 24, pp. 4794, 2022, DOI <https://doi.org/10.3390/math10244794>.
- <sup>62</sup>P. Livreri, E. Enrico, L. Fasolo, A. Greco, A. Rettaroli, D. Vitali, A. Farina, Com. F. Marchetti, and A. Sq. D. Giacomini, "Microwave Quantum Radar using a Josephson Traveling Wave Parametric Amplifier," 2022 IEEE Radar Conference (RadarConf22), 2022, pp. 1-5.
- <sup>63</sup>AB. Zorin, "Flux-driven Josephson traveling-wave parametric amplifier," *Phys. Rev. Appl.*, vol. 12, no. 4, pp. 044051, Oct. 2019, DOI 10.1103/PhysRevApplied.12.044051.
- <sup>64</sup>J. Mandula, J. Kühne, L. Pascarella, and M. Magno, "Towards real-time fast unmanned aerial vehicle detection using dynamic vision sensors," arXiv preprint arXiv:2403.11875, 2024, DOI <https://doi.org/10.48550/arXiv.2403.11875>.

- <sup>65</sup>P. Livreri, E. Enrico, D. Vitali, and A. Farina, "Microwave Quantum Radar using a Josephson Traveling Wave Parametric Amplifier and a Phase-Conjugate Receiver for a long-distance detection," 2023 IEEE Radar Conference (RadarConf23), San Antonio, TX, USA, 2023, pp. 1-5.
- <sup>66</sup>Z. Zhang, Y. Liu, T. Stephens, B. J. Eggleton, "Photonic radar for contactless vital sign detection," *Nature Photonics*, vol. 17, no. 9, pp. 791–797, 2023, DOI <https://doi.org/10.1038/s41566-023-01245-6>.
- <sup>67</sup>J. Gauthreaux, A. Sidney, and C. G. Belser, "Radar ornithology and biological conservation," *The Auk*, vol. 120, no. 2, pp. 266–277, 2003, DOI <https://doi.org/10.1093/auk/120.2.266>.
- <sup>68</sup>Lieutenant-Commander Graham Hill, "Quantum Radar Is Stealth Radar: Examining the Potential Impact on the Defence Team," Available: <https://www.cfc.forces.gc.ca/259/290/24/192/Hill>.
- <sup>69</sup>B. Balaji, M. Frasca and A. Farina, "Quantum Radar Research: A Snapshot in Time," *IEEE Aerospace and Electronic Systems Magazine*, vol. 35, no. 4, pp. 74-76, 2020, DOI 10.1109/MAES.2020.2977800.
- <sup>70</sup>J. B. Johnson, "Thermal agitation of electricity in conductors," *Physical review*, vol. 32, no. 1, pp. 97, 1928, DOI <https://doi.org/10.1103/PhysRev.32.97>.
- <sup>71</sup>N. Lauk, N. Sinclair, S. Barzanjeh, J. P. Covey, M. Saffman, M. Spiropulu, and C. Simon, "Perspectives on quantum transduction" *Quantum Science and Technology*, vol. 5, no. 2, pp. 020501, 2020, DOI 10.1088/2058-9565/ab788a.
- <sup>72</sup>H. Zhao, W. D. Chen, A. Kejriwal, and M. Mirhosseini, "Quantum-enabled microwave-to-optical transduction via silicon nanomechanics," *Nature Nanotechnology*, pp. 1–7, 2025, DOI <https://doi.org/10.1038/s41565-025-01874-8>.
- <sup>73</sup>Weedbrook, C., Pirandola, S., Thompson, J., Vedral, V. and Gu, M., "How discord underlies the noise resilience of quantum illumination," *New J. Phys.*, vol. 18, no. 4, pp. 043027, 2016. DOI 10.1088/1367-2630/18/4/043027.
- <sup>74</sup>Pirandola, S., Spedalieri, G., Braunstein, S.L., Cerf, N.J. and Lloyd, S., "Optimality of Gaussian discord," *Phys. Rev. Lett.*, vol. 113, no. 14, pp. 140405, 2014, DOI 10.1103/PhysRevLett.113.140405.
- <sup>75</sup>Devetak, Igor, and Andreas Winter, "Distilling common randomness from bipartite quantum states," *IEEE Trans. Inf. Theory*, vol. 50, no. 12, pp. 3183-3196, 2004, DOI 10.1109/TIT.2004.838115.
- <sup>76</sup>P. Ghelfi, F. Laghezza, F. Scotti, G. Serafino, A. Capria, S. Pinna, D. Onori, C. Porzi, M. Scaffardi, A. Malacarne, V. Vercesi, E. Lazzeri, F. Berizzi, and A. Bogoni, "A fully photonics-based coherent radar system," *Nat.*, vol. 507, no. 7492, pp. 341-345, 2014, DOI <https://doi.org/10.1038/nature13078>.
- <sup>77</sup>M. Bonaldi, A. Borrielli, G. Di Giuseppe, N. Malossi, B. Morana, R. Natali, P. Piergentili, P. M. Sarro, E. Serra, and D. Vitali "Low Noise Opto-Electro-Mechanical Modulator for RF-to-Optical Transduction in Quantum Communications," *Entropy*, vol. 25, no. 7, pp. 1087, 2023, DOI <https://doi.org/10.3390/e25071087>.
- <sup>78</sup>T. Gonzalez-Raya, and M. Sanz, "Coplanar antenna design for microwave entangled signals propagating in open air," *Quantum*, vol. 6, pp. 783, 2022, DOI 10.22331/q-2022-08-23-783.
- <sup>79</sup>P. Vezio, M. Bonaldi, A. Borrielli, F. Marino, B. Morana, P. M. Sarro, E. Serra, and F. Marin, "Optical self-cooling of a membrane oscillator in a cavity optomechanical experiment at room temperature," *Phys. Rev. A*, vol. 108, no. 10, pp. 063508, Dec 2023, DOI 10.1103/PhysRevA.108.063508.
- <sup>80</sup>G. Huang, A. Beccari, N. J. Engelsen, and T. J. Kippenberg, "Room-temperature quantum optomechanics using an ultralow noise cavity," *Nature*. 626, 512–516 (2024). DOI 10.1038/s41586-023-06997-3.
- <sup>81</sup>A. D'Elia, A. Rettaroli, F. Chiarello, D. Di Gioacchino, E. Enrico, L. Fasolo, C. Ligi, G. Maccarrone, F. Mantegazzini, B. Margesin, F. Mattioli, S. Tocci, A. Vinante and C. Gatti, "Microwave Photon Emission in Superconducting Circuits," *Instruments*, vol. 7, no. 4, 2023, DOI 10.3390/instruments7040036.
- <sup>82</sup>Ali Motazedifard, S. A. Madani, N. S. Vayaghan, "Measurement of entropy and quantum coherence properties of two type-I entangled photonic qubits," *Opt. Quant. Electron.*, vol. 53, no. 7, pp. 378, 2021, DOI <https://doi.org/10.1007/s11082-021-03384-y>.
- <sup>83</sup>Ali Motazedifard, S. A. Madani, J. J. Dashkasan, and N. S. Vayaghan, "Nonlocal realism tests and quantum state tomography in Sagnac-based type-II polarization-entanglement SPDC-source," *Heliyon*, vol. 7, no. 6, 2021, DOI <https://doi.org/10.1016/j.heliyon.2021.e07384>.
- <sup>84</sup>Ali Motazedifard and S. A. Madani "High-precision quantum transmittometry of DNA and methylene-blue using a frequency-entangled twin-photon beam in type-I SPDC," *OSA. Continuum.*, vol. 4, no. 3, pp. 1049-1069, 2021, DOI <https://doi.org/10.1364/OSAC.413830>.
- <sup>85</sup>H. Atarianpour, M. Hadian, M. Eskandari, A. Motazedifard, and R. Roknizadeh, "Quantum-Enhanced Radar based-on wideband NV-Center Receiver," *International Conference on Quantum Technologies and Industrial Applications at Shahid Beheshti University, Tehran, Iran May 28-May 29, 2024.*
- <sup>86</sup>Zh. Jiang, H. Cai, R. Cernansky, X. Liu, and W. Gao, "Quantum sensing of radio-frequency signal with NVcenters in SiC," *Sci. Adv.*, vol. 9, no. 20, pp. eadg2080, 2023, DOI 10.1126/sciadv.adg2080.
- <sup>87</sup>B. Zhang, Y. Han, H.-L. Wu, H. Wu, Sh. Yang, M. Oxborrow, Q. Zhao, Y. Fu, W. Li, Y. Wang, D. Zheng, and J. Zhang, "Ultra-sensitive solid-state organic molecular microwave quantum receiver," *arXiv:2405.15144v1 [quant-ph]* (2024). DOI 10.48550/arXiv.2405.15144
- <sup>88</sup>Sh. Zhang, Y. Liu, L. Shan, X. Gao, J. Geng, C. Yu, Y. Dong, X. Chen, G. Guo, and F. Sun, "Picotesla fiberized diamond-based AC magnetometer," *Photonics Research*. 12 (6), 1250 (2024). DOI 10.1364/PRJ.522062
- <sup>89</sup>K. Xu, Kai, Y. R. Zhang, Z. H. Sun, H. Li, P. Song, Z. Xiang, K. Huang, H. Li, Y. H. Shi, C. T. Chen, and others, "Metrological characterization of non-Gaussian entangled states of superconducting qubits," *Physical Review Letters*, vol. 128, no. 15, pp. 150501, 2022, DOI <https://doi.org/10.1103/PhysRevLett.128.150501>.
- <sup>90</sup>H. Zhang, Y. Xia, W. Ye, S. Chang, and Z. Liao, "Quantum illumination using non-Gaussian states with conditional measurements," *Physical Review A*, vol. 109, no. 6, pp. 062440, 2024, DOI <https://doi.org/10.1103/PhysRevA.109.062440>.
- <sup>91</sup>Tan, Si-Hui and Erkmen, Baris I and Giovannetti, Vittorio and Guha, Saikat and Lloyd, Seth and Maccone, Lorenzo and Pirandola, Stefano and Shapiro, Jeffrey H, "Quantum illumination with Gaussian states," *Phys. Rev. Lett.*, vol. 102, no. 25, pp. 253601, 2008, DOI 10.1103/PhysRevLett.101.253601.
- <sup>92</sup>J. Bourassa, and Ch. M. Wilson, "Progress Toward an All-Microwave Quantum Illumination Radar," *IEEE Aero. Electronic. Sys. Mag.* 35 (1)1, 58-69 (2020). DOI: 10.1109/MAES.2020.3024422.
- <sup>93</sup>C. Eichler, Y. Salathe, J. Mlynek, S. Schmidt, and A. Wallraff, "Quantum-limited amplification and entanglement in coupled nonlinear resonators," *Phys. Rev. Lett.* 113, 110502 (2014). DOI: 10.1103/PhysRevLett.113.110502
- <sup>94</sup>M. Lanzagorta, "Low-brightness quantum radar," *Proc. SPIE 9461, Radar Sensor Technology XIX; and Active and Passive Signatures*, vol. 9461, pp. 346-370, May 2015, DOI 10.1117/12.2177577.